

Hierarchical Nearest-Neighbor Gaussian Process Models for Large Geostatistical Datasets

Abhirup Datta, Sudipto Banerjee, Andrew O. Finley and Alan E. Gelfand

Abstract

Spatial process models for analyzing geostatistical data entail computations that become prohibitive as the number of spatial locations become large. This manuscript develops a class of highly scalable Nearest Neighbor Gaussian Process (NNGP) models to provide fully model-based inference for large geostatistical datasets. We establish that the NNGP is a well-defined spatial process providing legitimate finite-dimensional Gaussian densities with sparse precision matrices. We embed the NNGP as a dimension-reducing prior within a rich hierarchical modeling framework and develop computationally efficient Markov chain Monte Carlo (MCMC) algorithms avoiding the storage or decomposition of large matrices. The floating point operations (flops) per iteration of this algorithm is linear in the number of spatial locations, thereby delivering substantial scalability. We illustrate the computational and inferential benefits of the NNGP using simulation experiments and also infer on forest biomass from a massive United States Forest Inventory dataset.

KEYWORDS: Bayesian methods; composite likelihood; dimension reduction; hierarchical models; Markov chain Monte Carlo; nearest neighbors; predictive process; reduced-rank models; spatial cross-covariance functions.

1 Introduction.

With the advent of Geographical Information Systems (GIS), statisticians today routinely encounter geographically referenced datasets containing large number of irregularly located observations on multiple variables. This has, in turn, generated considerable interest in statistical modeling for location-referenced spatial data; see, for example, the books by Stein (1999), Moller and Waagepetersen (2003), Banerjee et al. (2014), Schabenberger and Gotway (2004), and Cressie and Wikle (2011) for a variety of methods and applications.

A typical approach assumes $\mathbf{y} \sim N(\mathbf{X}\boldsymbol{\beta}, \mathbf{C}(\boldsymbol{\theta}))$, where \mathbf{y} is an $n \times 1$ vector of spatially referenced observations, \mathbf{X} is a known $n \times p$ matrix of regressors and $\mathbf{C}(\boldsymbol{\theta})$ is a family of $n \times n$ covariance matrices indexed by an unknown set of parameters $\boldsymbol{\theta}$. When n is large and $\mathbf{C}(\boldsymbol{\theta})$ has no exploitable structure, evaluating the Gaussian log-likelihood becomes onerous because it involves the inverse and determinant of $\mathbf{C}(\boldsymbol{\theta})$. Numerically reliable matrix algorithms (e.g. Cholesky decomposition) require $\sim n^3$ floating point operations (flops) and storage of the

order of n^2 . These preclude exact evaluation of the log-likelihood on standard computing platforms when n is large. The cost is exacerbated because θ is unknown and needs to be estimated using an iterative procedure.

Broadly speaking, modeling large spatial datasets proceed by either exploiting “low-rank” models or using sparsity. The former develops representations of the spatial process on a lower-dimensional subspace (see, e.g., Higdon 2001; Kammann and Wand 2003; Stein 2007, 2008; Banerjee et al. 2008; Cressie and Johannesson 2008; Crainiceanu et al. 2008; Rasmussen and Williams 2005; Finley et al. 2009) by regressing the original (*parent*) process on its realizations over a smaller set of $r \ll n$ locations (“knots” or “centers”). Exploiting the low-rank structure reduces the algorithmic cost from $O(n^3)$ to $O(nr^2 + r^3) \approx O(nr^2)$ flops since $n \gg r$. However, when n is large, empirical investigations suggest that r must be fairly large to adequately approximate the parent process and the nr^2 flops becomes exorbitant in practice (see Section 5.1). More importantly, low rank models can provide poor likelihood approximations when neighboring observations are strongly correlated and the spatial signal dominates the noise (Stein 2013). Although modified low-rank models tend to perform much better (Finley et al. 2009; Banerjee et al. 2010; Sang and Huang 2012), these modifications can add to the computational burden and diminish scalability.

Methods exploiting sparse covariance structures include covariance tapering methods (see, e.g., Furrer et al. 2006; Kaufman et al. 2008; Du et al. 2009) or likelihood approximations using Markov random fields (e.g., Rue and Held 2004), a product of lower-dimensional conditional distributions (Vecchia 1988, 1992; Stein et al. 2004), or composite likelihoods (e.g., Eidsvik et al. 2014). The intuition behind these approaches is that spatial correlation between pairs of distantly located observations is nearly zero, so little information is lost in assuming conditional independence given intermediate locations. Covariance tapering can offer fully process-based inference but will require sparse determinant computations, which is awkward for large datasets. For most other sparse likelihood methods, inference has been restricted to finite sets of random variables and estimation and prediction have been based on likelihoods from different models. No underlying spatial process has been constructed to unify estimation, prediction (inference on uncountable sets) and model assessment.

This manuscript expands upon Vecchia (1988) and Stein et al. (2004) to show that likelihood approximations using lower-dimensional conditional distributions will yield proper densities under general conditions. More importantly, we show that these densities correspond to the distribution of finite-dimensional realizations of a well-defined spatial process, which we call the *Nearest-Neighbor Gaussian Process* (NNGP). The covariance matrix of its finite-dimensional realizations is sparse and delivers substantial computational gains. Like the low rank predictive process, working with a well-defined spatial process, rather than a likelihood approximation, provides a unified framework for estimation, prediction, model comparison and, in particular, enables inference on arbitrary sets of random variables. Unlike low-rank processes, the NNGP does not produce degenerate finite dimensional realizations and produces substantial computational and inferential benefits over low rank processes. Rather than dimension reduction, the NNGP exploits matrix sparsity in a fully process-based framework.

To demonstrate the full inferential capabilities of the NNGP, we adopt a Bayesian mod-

eling framework using well-defined posterior predictive distributions. In particular, we carry out fully model-based inference for the entire spatial residual surface after accounting for predictors to discern residual spatial patterns. We can evaluate the performance of all NNGP models using standard model comparison techniques, circumventing the need to invoke possibly inappropriate asymptotic results involving restricted likelihoods and estimating equations. From an implementation standpoint, we develop a very efficient Gibbs sampling algorithm that avoids storage and computations involving large matrices.

The article evolves as follows. Section 2 formulates the NNGP using multivariate Gaussian processes. Section 3 outlines Bayesian estimation and prediction for these models within a very flexible hierarchical modeling setup. Section 4 discusses alternative NNGP models and algorithms. Section 5 illustrates with simulation and forestry data analysis. Finally, Section 6 concludes the manuscript with a brief summary and pointers toward future work.

2 Nearest-Neighbor Gaussian Process

2.1 A nearest-neighbor multivariate Gaussian density

Let $\mathbf{w}(\mathbf{s}) \sim GP(\mathbf{0}, \mathbf{C}(\cdot, \cdot | \boldsymbol{\theta}))$ denote a zero-centered q -variate Gaussian process, where $\mathbf{w}(\mathbf{s}) \in \Re^{q \times 1}$ for all $\mathbf{s} \in \mathcal{D} \subseteq \Re^d$. The process is completely specified by a valid cross-covariance function $\mathbf{C}(\cdot, \cdot | \boldsymbol{\theta})$, which maps a pair of locations \mathbf{s} and \mathbf{t} in $\mathcal{D} \times \mathcal{D}$ into a $q \times q$ real valued matrix $\mathbf{C}(\mathbf{s}, \mathbf{t})$ with entries $\text{cov}\{w_i(\mathbf{s}), w_j(\mathbf{t})\}$. Here, $\boldsymbol{\theta}$ denotes the parameters associated with the cross-covariance function. Let $\mathcal{S} = \{\mathbf{s}_1, \mathbf{s}_2, \dots, \mathbf{s}_k\}$ be a fixed finite collection of locations in \mathcal{D} which we call the *reference set*. If A is any finite collection of locations, \mathbf{w}_A will denote the column vector formed by stacking the realizations of $\mathbf{w}(\mathbf{s})$ over A . So, $\mathbf{w}_{\mathcal{S}} \sim N(\mathbf{0}, \mathbf{C}_{\mathcal{S}}(\boldsymbol{\theta}))$, where $\mathbf{w}_{\mathcal{S}} = (\mathbf{w}(\mathbf{s}_1)', \mathbf{w}(\mathbf{s}_2)', \dots, \mathbf{w}(\mathbf{s}_k)')$ and $\mathbf{C}_{\mathcal{S}}(\boldsymbol{\theta})$ is a positive definite $qk \times qk$ block matrix with $\mathbf{C}(\mathbf{s}_i, \mathbf{s}_j)$ as its blocks. Henceforth, we write $\mathbf{C}_{\mathcal{S}}(\boldsymbol{\theta})$ as $\mathbf{C}_{\mathcal{S}}$, ignoring the implicit dependence on $\boldsymbol{\theta}$, with similar notation for all spatial covariance matrices. Given any ordering of the locations, the joint density of \mathbf{w} can be written as $p(\mathbf{w}) = \prod_{i=1}^k p(\mathbf{w}(\mathbf{s}_i) | \mathbf{w}_{<i})$, where $\mathbf{w}_{<i} = (\mathbf{w}(\mathbf{s}_1)', \mathbf{w}(\mathbf{s}_2)', \dots, \mathbf{w}(\mathbf{s}_{(i-1)})')$ is $(i-1)q \times 1$ for $2 \leq i \leq n$ and is empty when $i = 1$.

When k is large, the conditioning sets $\mathbf{w}_{<i}$ are also very large for i close to k . To achieve dimension reduction, we do not consider the full conditioning sets $\mathbf{w}_{<i}$. Instead, for every $\mathbf{s}_i \in \mathcal{S}$ we define a smaller set $N(\mathbf{s}_i) \subset \mathcal{S} \setminus \{\mathbf{s}_i\}$ consisting of “neighbors” of \mathbf{s}_i . The term “neighbor” is loosely defined as of now and can be specified by the user as we discuss below. Let $\mathbf{w}_{N(\mathbf{s}_i)}$ be the vector formed by stacking the realizations of $\mathbf{w}(\mathbf{s})$ over $N(\mathbf{s}_i)$. We replace $\mathbf{w}_{<i}$ with $\mathbf{w}_{N(\mathbf{s}_i)}$ in the conditional densities to obtain the composite likelihood

$$\tilde{p}(\mathbf{w}_{\mathcal{S}}) = \prod_{i=1}^k p(\mathbf{w}(\mathbf{s}_i) | \mathbf{w}_{N(\mathbf{s}_i)}) . \quad (1)$$

Let $N_{\mathcal{S}} = \{N(\mathbf{s}_i); i = 1, 2, \dots, k\}$ be the collection of all neighbor sets over \mathcal{S} . We can view the pair $\{\mathcal{S}, N_{\mathcal{S}}\}$ as a directed graph \mathcal{G} with vertices at $\mathbf{s}_1, \mathbf{s}_2, \dots, \mathbf{s}_k$ and directed edges to every vertex \mathbf{s}_i from all locations in $N(\mathbf{s}_i)$. The following Theorem states that \tilde{p} in (1) is

a valid joint distribution for \mathbf{w}_S under very general assumptions on the neighbor sets. We postpone this proof, and all subsequent proofs, to the Appendix.

Theorem 1 *Let $\mathcal{S} = \{\mathbf{s}_1, \mathbf{s}_2, \dots, \mathbf{s}_k\}$ denote a finite set and $(\mathbf{w}(\mathbf{s}_1)', \mathbf{w}(\mathbf{s}_2)', \dots, \mathbf{w}(\mathbf{s}_k)')$ be a random vector over \mathcal{S} with density $p(\mathbf{w}_S)$. For every $\mathbf{s}_i \in \mathcal{S}$, let $N(\mathbf{s}_i)$ denote a subset of $\mathcal{S} \setminus \{\mathbf{s}_i\}$. Let \mathcal{G} be the directed graph formed with vertices \mathbf{s}_i and directed edges to \mathbf{s}_i from all elements in $N(\mathbf{s}_i)$. If \mathcal{G} is acyclic then $\tilde{p}(\mathbf{w}_S)$ given by (1) is a valid joint density.*

Theorem 1 ensures that any collection N_S which forms an acyclic directed graph \mathcal{G} is a legitimate choice for neighbors. A sufficient condition is to let $N(\mathbf{s}_i)$ be a subset of the “past” locations $\mathcal{S}_i = \{\mathbf{s}_1, \mathbf{s}_2, \dots, \mathbf{s}_{i-1}\}$. A natural premise for specifying N_S is that spatial correlations are strongest between nearby locations and they diminish for locations farther apart. Stein et al. (2004) points out some caveats and considers near and as well as a few far points but always from the past. So, his choices also ensure an acyclic specification.

One natural choice for these subsets is based upon m -nearest neighbors from the past in terms of Euclidean distance, where m is much smaller than k . To be specific, let

$$N(\mathbf{s}_i) = \begin{cases} \text{empty set for } i = 1 \\ \{\mathbf{s}_1, \mathbf{s}_2, \dots, \mathbf{s}_{i-1}\} \text{ for } 2 \leq i \leq m \\ m \text{ nearest neighbors of } \mathbf{s}_i \text{ among } \{\mathbf{s}_1, \mathbf{s}_2, \dots, \mathbf{s}_{i-1}\} \text{ for } i > m \end{cases} \quad (2)$$

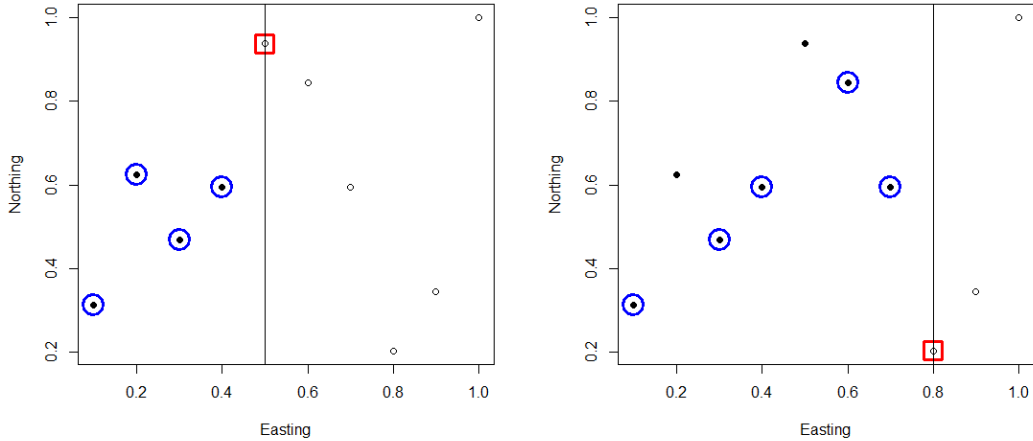
The resulting $\tilde{p}(\mathbf{w}_S)$ reduces to the approximate likelihood used by Vecchia (1988) and is, from Theorem 1, again a proper density from a different model. Figure 1 illustrates how we construct these neighborhood sets for each point. The $N(\mathbf{s}_i)$ ’s depend upon the ordering imposed on \mathcal{S} . While it might be tempting to choose m -nearest neighbors instead of m -nearest neighbors *from the past*, all such order-free choices of neighbor sets destroy the acyclic property and do not produce valid densities. Also, for any ordering $\tilde{p}(\mathbf{w}_S)$ approaches the true density $p(\mathbf{w}_S)$ as m approaches k . So, we assume that \mathcal{S} is a fixed set of locations with some predetermined ordering (e.g. along one of the coordinates).

Models based on past neighbors are common in time series settings, where time points are naturally ordered. There, the obvious choice for neighbor is the last m time points leading to an autoregressive (AR(m)) model. In spatial settings, the locations are not naturally ordered which necessitates a predetermined collection of neighbor sets to construct the model. For convenience our subsequent developments are based on $N(\mathbf{s}_i)$ ’s defined in (2) although the theory is valid as long as $N(\mathbf{s}_i)$ is any subset of \mathcal{S}_i of size at most m . These choices for the $N(\mathbf{s}_i)$ ’s retain the acyclic structure and are particular cases of this general framework.

While Theorem 1 holds for any density $p(\mathbf{w}_S)$, here we assume it is the density of the realizations of a Gaussian process over \mathcal{S} with cross covariance function $\mathbf{C}(\cdot, \cdot)$. Let $\mathbf{C}_{N(\mathbf{s}_i)}$ be the $m q \times m q$ covariance matrix of $\mathbf{w}_{N(\mathbf{s}_i)}$ and let $\mathbf{C}_{\mathbf{s}_i, N(\mathbf{s}_i)}$ be the $q \times m q$ cross-covariance matrix between the random vectors $\mathbf{w}(\mathbf{s}_i)$ and $\mathbf{w}_{N(\mathbf{s}_i)}$. Standard distribution theory implies that $p(\mathbf{w}(\mathbf{s}_i) | \mathbf{w}_{N(\mathbf{s}_i)}) = N(\mathbf{w}(\mathbf{s}_i) | \mathbf{B}_{\mathbf{s}_i} \mathbf{w}_{N(\mathbf{s}_i)}, \mathbf{F}_{\mathbf{s}_i})$ where,

$$\mathbf{B}_{\mathbf{s}_i} = \mathbf{C}_{\mathbf{s}_i, N(\mathbf{s}_i)} \mathbf{C}_{N(\mathbf{s}_i)}^{-1} \text{ and } \mathbf{F}_{\mathbf{s}_i} = \mathbf{C}(\mathbf{s}_i, \mathbf{s}_i) - \mathbf{C}_{\mathbf{s}_i, N(\mathbf{s}_i)} \mathbf{C}_{N(\mathbf{s}_i)}^{-1} \mathbf{C}_{N(\mathbf{s}_i), \mathbf{s}_i} \cdot \quad (3)$$

Theorem 2 states that $\tilde{p}(\mathbf{w}_S)$ is a Gaussian density with a sparse precision matrix.



(a) Neighbors for $i = 5$

(b) Neighbors for $i = 8$

Figure 1: Figures (a) and (b) illustrates the construction of neighbor sets for an NNGP process with $m=5$ for a toy dataset with 10 observations. Filled circles identify the set of possible neighbors of \mathbf{s}_i (the red square). When we order observations by their x -coordinate, this set of possible neighbors are all observations left of the vertical line. The neighbors of \mathbf{s}_i are identified by blue circles. Open circle symbols, i.e., all locations to the right of the vertical line, represent those locations not in set \mathcal{S}_i .

Theorem 2 (a) If $p(\mathbf{w}_S) = N(\mathbf{w}_S | \mathbf{0}, \mathbf{C}_S)$, then $\tilde{p}(\mathbf{w}_S) = N(\mathbf{w}_S | \mathbf{0}, \tilde{\mathbf{C}}_S)$, where $\tilde{\mathbf{C}}_S = (\mathbf{B}_S \mathbf{F}_S^{-1} \mathbf{B}_S)^{-1}$, \mathbf{F}_S is block diagonal with i^{th} block $\mathbf{F}_{\mathbf{s}_i}$ and \mathbf{B}_S is lower triangular.

(b) For $m \ll k$, $\tilde{\mathbf{C}}_S^{-1}$ is a sparse matrix with at most $km(m+1)q^2/2$ non-zero entries

The proof and the precise structure of \mathbf{B}_S is provided in Appendix A. Given the parent model $N(\mathbf{0}, \mathbf{C}_S)$, we have derived a new Gaussian model $\mathbf{w}_S \sim N(\mathbf{0}, \tilde{\mathbf{C}}_S)$ with a sparse precision matrix. This can be regarded as the spatial analogue of an autoregressive time series model with a band-diagonal precision matrix. The sparsity pattern of $\tilde{\mathbf{C}}_S^{-1}$ depends upon the neighborhood structure N_S which in turn depends on the ordering of the data and the size m of the neighbor sets. Figure 2 shows how the sparsity pattern of $\tilde{\mathbf{C}}_S^{-1}$ varies for the same \mathcal{S} but with different m and ordering. Under this new model, the likelihood $\tilde{p}(\mathbf{w}_S)$ is computationally much more tractable than $p(\mathbf{w}_S)$ for large k . We call $\tilde{p}(\mathbf{w}_S)$ the “nearest neighbor density” for \mathbf{w}_S .

We distinguish the above formulation from some composite likelihood approaches which do not necessarily yield valid probability densities. For us replacing $\mathbf{w}_{<i}$ with $\mathbf{w}_{N(\mathbf{s}_i)}$ corresponds to a true density from a different probability model for a varied choice of neighborhood sets. This allows us to compare the parent model with a nearest neighbor Gaussian model using standard model comparison techniques without invoking any results for composite or

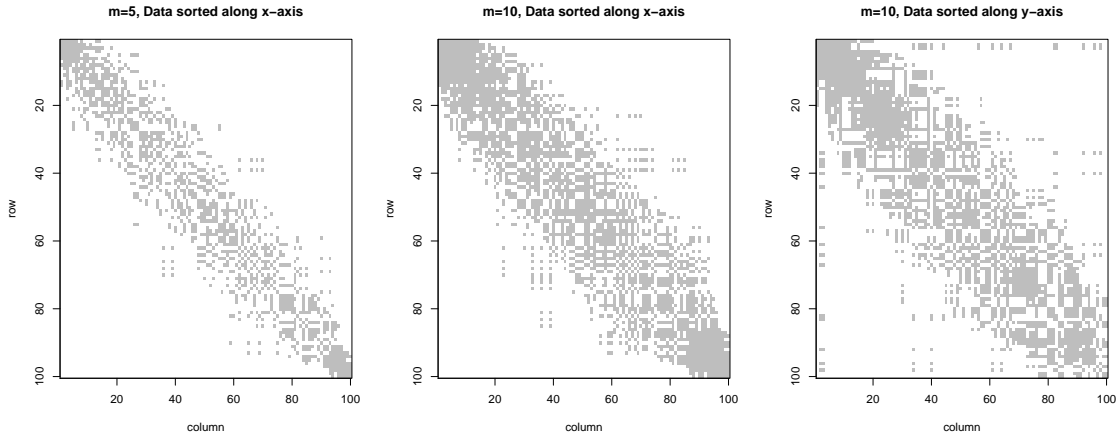


Figure 2: The sparsity patterns of NNGP precision matrices for different choices of m and ordering of the data. 100 locations were generated on the x-y plane from $N(0, 1) \times N(0, 1)$. The x-coordinate of 5 random locations were given a jump of 10. The correlation structure for the parent process was chosen from the univariate Matérn family defined in (12) with $\nu = 0.5, \phi = 3.5$ and variances were chosen to be 1.0

pseudo-likelihoods. Also, $\mathbf{w}_{\mathcal{S}} \sim N(\mathbf{0}, \tilde{\mathbf{C}}_{\mathcal{S}})$ can be seamlessly embedded in any hierarchical spatial regression setup to obtain sample-based inference from the posterior distribution without any computational roadblocks (see Section 3).

2.2 A Nearest-Neighbor Spatial Process

If \mathcal{S} is not fixed at the outset, then inference at arbitrary locations may not be consistent. To elucidate, let us assume that the elements of \mathcal{S} are ordered along the x -axis. Consider a new location \mathbf{s}_0 . If we rearrange $\{\mathbf{s}_0, \mathbf{s}_1, \dots, \mathbf{s}_k\}$ based on their x -coordinates, then the neighbor sets $N_{\mathcal{S}}$ may change and, consequently, the new $\tilde{p}(\mathbf{w}_{\mathcal{S}})$ obtained by integrating out $\mathbf{w}(\mathbf{s}_0)$ from $\tilde{p}(\mathbf{w}_{\mathcal{S}}, \mathbf{w}(\mathbf{s}_0))$ may not be the same as the original $\tilde{p}(\mathbf{w}_{\mathcal{S}})$. Therefore, to construct a spatial process we must keep the reference set \mathcal{S} fixed.

First consider any location \mathbf{u} outside \mathcal{S} . Consistent with the definition of $N(\mathbf{s}_i)$, let $N(\mathbf{u})$ be the set of m -nearest neighbors of \mathbf{u} in \mathcal{S} . Hence, for any finite set $\mathcal{U} = \{\mathbf{u}_1, \mathbf{u}_2, \dots, \mathbf{u}_r\}$ such that $\mathcal{S} \cap \mathcal{U}$ is empty, we define the nearest neighbor density of $\mathbf{w}_{\mathcal{U}}$ conditional on $\mathbf{w}_{\mathcal{S}}$ as

$$\tilde{p}(\mathbf{w}_{\mathcal{U}} | \mathbf{w}_{\mathcal{S}}) = \prod_{i=1}^r p(\mathbf{w}(\mathbf{u}_i) | \mathbf{w}_{N(\mathbf{u}_i)}) . \quad (4)$$

This conditional density is akin to (1) except that all the neighbor sets are subset of \mathcal{S} . This ensures a proper conditional density. Indeed (1) and (4) are sufficient to describe the joint density of *any* finite set over the domain \mathcal{D} . More precisely, if $\mathcal{V} = \{\mathbf{v}_1, \mathbf{v}_2, \dots, \mathbf{v}_n\}$ is *any*

finite subset in \mathcal{D} , then, using (4) we obtain the density of $\mathbf{w}_{\mathcal{V}}$ as,

$$\tilde{p}(\mathbf{w}_{\mathcal{V}}) = \int \tilde{p}(\mathbf{w}_{\mathcal{U}} | \mathbf{w}_{\mathcal{S}}) \tilde{p}(\mathbf{w}_{\mathcal{S}}) \prod_{\{\mathbf{s}_i \in \mathcal{S} \setminus \mathcal{V}\}} d(\mathbf{w}(\mathbf{s}_i)) \quad \text{where } \mathcal{U} = \mathcal{V} \setminus \mathcal{S}. \quad (5)$$

If \mathcal{U} is empty, then (4) implies that $\tilde{p}(\mathbf{w}_{\mathcal{U}} | \mathbf{w}_{\mathcal{S}}) = 1$ in (5). If $\mathcal{S} \setminus \mathcal{V}$ is empty, then the integration in (5) is not needed.

Theorem 3 establishes that these probability densities, defined on finite topologies, conform to Kolmogorov's consistency criteria and, hence, correspond to a valid spatial process over \mathcal{D} . We refer to this as a *Nearest Neighbor Process*.

Theorem 3 *Let $\{\mathbf{w}(\mathbf{s}) | \mathbf{s} \in \mathcal{D}\}$ be a random process over some domain \mathcal{D} with density p and let $\tilde{p}(\mathbf{w}_{\mathcal{S}})$ be a probability density for observations over a fixed finite set $\mathcal{S} \subset \mathcal{D}$. If we define the conditional density $\tilde{p}(\mathbf{w}_{\mathcal{U}} | \mathbf{w}_{\mathcal{S}})$ for any finite set $\mathcal{U} \subset \mathcal{D}$ outside of \mathcal{S} , as in (4), then the probability densities \tilde{p} defined in (5) satisfy Kolmogorov's consistency criteria.*

(a) *For every finite set $\mathcal{V} = \{\mathbf{v}_1, \mathbf{v}_2, \dots, \mathbf{v}_n\}$ in \mathcal{D} , $n \in \{1, 2, \dots\}$ and for every permutation $\pi(1), \pi(2), \dots, \pi(n)$ of $1, 2, \dots, n$ we have,*

$$\tilde{p}(\mathbf{w}(\mathbf{v}_1), \mathbf{w}(\mathbf{v}_2), \dots, \mathbf{w}(\mathbf{v}_n)) = \tilde{p}(\mathbf{w}(\mathbf{v}_{\pi(1)}), \mathbf{w}(\mathbf{v}_{\pi(2)}), \dots, \mathbf{w}(\mathbf{v}_{\pi(n)})) .$$

(b) *For every location $\mathbf{v}_0 \in \mathcal{D}$, we have, $\tilde{p}(\mathbf{w}_{\mathcal{V}}) = \int \tilde{p}(\mathbf{w}_{\mathcal{V} \cup \{\mathbf{v}_0\}}) d(\mathbf{w}(\mathbf{v}_0))$.*

So, given any original (parent) spatial process and any *fixed* reference set \mathcal{S} , we can construct a new process over the domain \mathcal{D} using a collection of neighbor sets in \mathcal{S} . We show in Theorem 4 that any finite dimensional distribution for a nearest neighbor spatial process derived from a parent Gaussian process will be Gaussian.

Theorem 4 *Let the parent process be a stationary Gaussian process, $GP(\boldsymbol{\theta}, \mathbf{C}(\cdot, \cdot | \boldsymbol{\theta}))$.*

(a) *For any finite set $\mathcal{U} = \{\mathbf{u}_1, \mathbf{u}_2, \dots, \mathbf{u}_r\}$ in \mathcal{D} outside \mathcal{S} let $\mathbf{B}_{\mathbf{u}_i}$ and $\mathbf{F}_{\mathbf{u}_i}$ be defined analogous to (3) based on the neighbor sets $N(\mathbf{u}_i)$. Then,*

$$\tilde{p}(\mathbf{w}_{\mathcal{U}} | \mathbf{w}_{\mathcal{S}}) = \prod_{i=1}^r N(\mathbf{w}(\mathbf{u}_i) | \mathbf{B}_{\mathbf{u}_i} \mathbf{w}_{N(\mathbf{u}_i)}, \mathbf{F}_{\mathbf{u}_i}) = N(\mathbf{B}_{\mathcal{U}} \mathbf{w}_{\mathcal{S}}, \mathbf{F}_{\mathcal{U}}) \quad (6)$$

where $\mathbf{F}_{\mathcal{U}} = \text{diag}(\mathbf{F}_{\mathbf{u}_1}, \mathbf{F}_{\mathbf{u}_2}, \dots, \mathbf{F}_{\mathbf{u}_r})$ and $\mathbf{B}_{\mathcal{U}}$ is a sparse $nq \times kq$ matrix with each row having at most mq non-zero entries.

(b) *For any finite set \mathcal{V} in \mathcal{D} , $\tilde{p}(\mathbf{w}_{\mathcal{V}})$ is the density arising from a finite dimensional Gaussian process with cross covariance function*

$$\tilde{\mathbf{C}}(\mathbf{v}_1, \mathbf{v}_2; \boldsymbol{\theta}) = \begin{cases} \tilde{\mathbf{C}}_{\mathbf{s}_i, \mathbf{s}_j}, & \text{if } \mathbf{v}_1 = \mathbf{s}_i \text{ and } \mathbf{v}_2 = \mathbf{s}_j \text{ are both in } \mathcal{S}, \\ \mathbf{B}_{\mathbf{v}_1} \tilde{\mathbf{C}}_{N(\mathbf{v}_2), \mathbf{s}_j} & \text{if } \mathbf{v}_1 \notin \mathcal{S} \text{ and } \mathbf{v}_2 = \mathbf{s}_j \in \mathcal{S}, \\ \mathbf{B}_{\mathbf{v}_1} \tilde{\mathbf{C}}_{N(\mathbf{v}_1), N(\mathbf{v}_2)} \mathbf{B}'_{\mathbf{v}_2} + \delta_{(\mathbf{v}_1 = \mathbf{v}_2)} \mathbf{F}_{\mathbf{v}_1} & \text{if } \mathbf{v}_1 \text{ and } \mathbf{v}_2 \text{ are not in } \mathcal{S} \end{cases} \quad (7)$$

where \mathbf{v}_1 and \mathbf{v}_2 are any two locations in \mathcal{D} , $\tilde{\mathbf{C}}_{A,B}$ denotes submatrices of $\tilde{\mathbf{C}}_{\mathcal{S}}$ indexed by the locations in the sets A and B , and $\delta_{(\mathbf{v}_1=\mathbf{v}_2)}$ is the Kronecker delta.

(c) $\tilde{\mathbf{C}}(\mathbf{v}_1, \mathbf{v}_2 | \boldsymbol{\theta})$ is continuous for all \mathbf{v}_1 and \mathbf{v}_2 such that $\mathbf{v}_1 \neq \mathbf{v}_2$.

The preceding theorems ensure the existence of a well-defined *Nearest Neighbor Gaussian Process*, $NNGP(\mathbf{0}, \tilde{\mathbf{C}}(\cdot, \cdot | \boldsymbol{\theta}))$, derived from a *parent Gaussian process*, $GP(\mathbf{0}, \mathbf{C}(\cdot, \cdot | \boldsymbol{\theta}))$. The conditional distribution of $\mathbf{w}_{\mathcal{U}} | \mathbf{w}_{\mathcal{S}}$ somewhat resembles that in low-rank processes, where \mathcal{S} is the set of “knots” and smaller number of knots, i.e., $k \ll n$, ensures dimension reduction. In the NNGP, k can be as large, or even larger, than n and the reduction in computational complexity is achieved through sparsity of NNGP covariance matrices. In other words, the NNGP is *not* a singular process as arises with customary dimension reduction approaches which confine the process to a finite dimensional space.

3 Bayesian estimation and implementation.

3.1 A hierarchical model.

Flexible multivariate geostatistical models envision a vector of l dependent variables, say $\mathbf{y}(\mathbf{t})$, at location $\mathbf{t} \in \mathcal{D} \subseteq \mathbb{R}^d$ in a spatially-varying regression model,

$$\mathbf{y}(\mathbf{t}) = \mathbf{X}(\mathbf{t})' \boldsymbol{\beta} + \mathbf{Z}(\mathbf{t})' \mathbf{w}(\mathbf{t}) + \boldsymbol{\epsilon}(\mathbf{t}), \quad (8)$$

where $\mathbf{X}(\mathbf{t})'$ is the $l \times p$ matrix of fixed spatially-referenced predictors, $\mathbf{w}(\mathbf{t})$ is a $q \times 1$ spatial process forming the coefficients of the $l \times q$ fixed design matrix $\mathbf{Z}(\mathbf{t})'$, and $\boldsymbol{\epsilon}(\mathbf{t}) \stackrel{iid}{\sim} N(\mathbf{0}, \mathbf{D})$ is an $l \times 1$ white noise process capturing measurement error or micro-scale variability with dispersion matrix \mathbf{D} , which we assume is diagonal with entries τ_j^2 , $j = 1, 2, \dots, l$. The matrix $\mathbf{X}(\mathbf{t})'$ is block diagonal with $p = \sum_{i=1}^l p_i$, where the $1 \times p_i$ vector $\mathbf{x}_i(\mathbf{t})'$, including perhaps an intercept, is the i -th block for each $i = 1, 2, \dots, l$. The model in (8) subsumes several specific spatial models. For instance, letting $q = l$ and $\mathbf{Z}(\mathbf{t})' = \mathbf{I}_{l \times l}$ leads to a multivariate spatial regression model where $\mathbf{w}(\mathbf{t})$ acts as a *spatially-varying intercept*. On the other hand, we could envision all coefficients to be spatially-varying and set $q = p$ with $\mathbf{Z}(\mathbf{t})' = \mathbf{X}(\mathbf{t})'$. With $l = 1$, we obtain their univariate analogues.

For dimension reduction, instead of a customary Gaussian process prior for $\mathbf{w}(\mathbf{t})$ in (8), we assume $\mathbf{w}(\mathbf{t}) \sim NNGP(\mathbf{0}, \tilde{\mathbf{C}}(\cdot, \cdot | \boldsymbol{\theta}))$ induced by the parent process $GP(\mathbf{0}, \mathbf{C}(\cdot, \cdot | \boldsymbol{\theta}))$. Any valid stationary cross covariance function (see, e.g., Gelfand and Banerjee 2010) can be used to construct $\mathbf{C}(\cdot, \cdot | \boldsymbol{\theta})$. To elucidate, let $\mathcal{T} = \{\mathbf{t}_1, \mathbf{t}_2, \dots, \mathbf{t}_n\}$ be the set of locations where the outcomes and predictors have been observed. This set may or may not intersect with the reference set used to construct the NNGP. If $\mathcal{S} = \{\mathbf{s}_1, \mathbf{s}_2, \dots, \mathbf{s}_k\}$ is the reference set for the NNGP, then, without loss of generality we split up \mathcal{T} into \mathcal{S}^* and \mathcal{U} where $\mathcal{S}^* = \mathcal{S} \cap \mathcal{T} = \{\mathbf{s}_{i_1}, \mathbf{s}_{i_2}, \dots, \mathbf{s}_{i_r}\}$ with $\mathbf{s}_{i_j} = \mathbf{t}_j$ for $j = 1, 2, \dots, r$ and $\mathcal{U} = \mathcal{T} \setminus \mathcal{S} = \{\mathbf{t}_{r+1}, \mathbf{t}_{r+2}, \dots, \mathbf{t}_n\}$. Since $\mathcal{S} \cup \mathcal{T} = \mathcal{S} \cup \mathcal{U}$, Theorems 2 and 4 enable us to completely specify the realizations of the NNGP in terms of the realizations of the parent process over \mathcal{S} and \mathcal{U} , hierarchically, as $\mathbf{w}_{\mathcal{U}} | \mathbf{w}_{\mathcal{S}} \sim N(\mathbf{B}_{\mathcal{U}} \mathbf{w}_{\mathcal{S}}, \mathbf{F}_{\mathcal{U}})$ and $\mathbf{w}_{\mathcal{S}} \sim N(\mathbf{0}, \tilde{\mathbf{C}}_{\mathcal{S}})$. For a full Bayesian specification, we

further specify prior distributions on $\boldsymbol{\beta}$, $\boldsymbol{\theta}$ and the τ_j^2 's. For example, with customary prior specifications, we obtain the joint distribution

$$p(\boldsymbol{\theta}) \times \prod_{j=1}^q IG(\tau_j^2 | a_{\tau_j}, b_{\tau_j}) \times N(\boldsymbol{\beta} | \boldsymbol{\mu}_\beta, \mathbf{V}_\beta) \times N(\mathbf{w}_U | \mathbf{B}_U \mathbf{w}_S, \mathbf{F}_U) \\ \times N(\mathbf{w}_S | \mathbf{0}, \tilde{\mathbf{C}}_S) \times \prod_{i=1}^n N(\mathbf{y}(\mathbf{t}_i) | \mathbf{X}(\mathbf{t}_i)' \boldsymbol{\beta} + \mathbf{Z}(\mathbf{t}_i)' \mathbf{w}(\mathbf{t}_i), \mathbf{D}), \quad (9)$$

where $p(\boldsymbol{\theta})$ is the prior on $\boldsymbol{\theta}$ and $IG(\tau_j^2 | a_{\tau_j}, b_{\tau_j})$ denotes the Inverse-Gamma density.

3.2 Estimation and prediction.

To describe a Gibbs sampler for estimating (9), we define $\mathbf{y} = (\mathbf{y}(\mathbf{t}_1)', \mathbf{y}(\mathbf{t}_2)', \dots, \mathbf{y}(\mathbf{t}_n)')'$, and \mathbf{w} and $\boldsymbol{\epsilon}$ similarly. Also, we introduce $\mathbf{X} = [\mathbf{X}(\mathbf{t}_1) : \mathbf{X}(\mathbf{t}_2) : \dots : \mathbf{X}(\mathbf{t}_n)]'$, $\mathbf{Z} = \text{diag}(\mathbf{Z}(\mathbf{t}_1)', \dots, \mathbf{Z}(\mathbf{t}_n)')$, and $\mathbf{D}_n = \text{Cov}(\boldsymbol{\epsilon}) = \text{diag}(\mathbf{D}, \dots, \mathbf{D})$. The full conditional distribution for $\boldsymbol{\beta}$ is $N(\mathbf{V}_\beta^* \boldsymbol{\mu}_\beta^*, \mathbf{V}_\beta^*)$, where $\mathbf{V}_\beta^* = (\mathbf{V}_\beta^{-1} + \mathbf{X}' \mathbf{D}_n^{-1} \mathbf{X})^{-1}$, $\boldsymbol{\mu}_\beta^* = (\mathbf{V}_\beta^{-1} \boldsymbol{\mu}_\beta + \mathbf{X}' \mathbf{D}_n^{-1} (\mathbf{y} - \mathbf{Z} \mathbf{w}))$. Inverse-Gamma priors for the τ_j^2 's leads to conjugate full conditional distribution $IG(a_{\tau_j} + \frac{n}{2}, b_{\tau_j} + \frac{1}{2}(\mathbf{y}_{*j} - \mathbf{X}_{*j} \boldsymbol{\beta} - \mathbf{Z}_{*j} \mathbf{w})'(\mathbf{y}_{*j} - \mathbf{X}_{*j} \boldsymbol{\beta} - \mathbf{Z}_{*j} \mathbf{w}))$ where \mathbf{y}_{*j} refers to the $n \times 1$ vector containing the j^{th} co-ordinates of the $\mathbf{y}(\mathbf{t}_i)$'s, \mathbf{X}_{*j} and \mathbf{Z}_{*j} are the corresponding fixed and spatial effect covariate matrices respectively. For updating $\boldsymbol{\theta}$, we use a Metropolis step with target density $p(\boldsymbol{\theta}) \times N(\mathbf{w}_S | \mathbf{0}, \tilde{\mathbf{C}}_S) \times N(\mathbf{w}_U | \mathbf{B}_U \mathbf{w}_S, \mathbf{F}_U)$, where

$$N(\mathbf{w}_S | \mathbf{0}, \tilde{\mathbf{C}}_S) = \prod_{i=1}^k N(\mathbf{w}(\mathbf{s}_i) | \mathbf{B}_{\mathbf{s}_i} \mathbf{w}_{N(\mathbf{s}_i)}, \mathbf{F}_{\mathbf{s}_i}) \text{ and} \\ N(\mathbf{w}_U | \mathbf{B}_U \mathbf{w}_S, \mathbf{F}_U) = \prod_{i=r+1}^n N(\mathbf{w}(\mathbf{t}_i) | \mathbf{B}_{\mathbf{t}_i} \mathbf{w}_{N(\mathbf{t}_i)}, \mathbf{F}_{\mathbf{t}_i}) \quad (10)$$

Each of the component densities under the product sign on the right hand side of (10) can be evaluated without any n -dimensional matrix operations rendering the NNGP suitable for efficient Metropolis (Hastings) block updates for $\boldsymbol{\theta}$.

Since the components of $\mathbf{w}_U | \mathbf{w}_S$ are independent, we can update $\mathbf{w}(\mathbf{t}_i)$ from its full conditional $N(\mathbf{V}_{\mathbf{t}_i} \boldsymbol{\mu}_{\mathbf{t}_i}, \mathbf{V}_{\mathbf{t}_i})$ for $i = r+1, r+2, \dots, n$ where $\mathbf{V}_{\mathbf{t}_i} = (\mathbf{Z}(\mathbf{t}_i) \mathbf{D}^{-1} \mathbf{Z}(\mathbf{t}_i)' + \mathbf{F}_{\mathbf{t}_i}^{-1})^{-1}$ and $\boldsymbol{\mu}_{\mathbf{t}_i} = \mathbf{Z}(\mathbf{t}_i) \mathbf{D}^{-1} (\mathbf{y}(\mathbf{t}_i) - \mathbf{X}(\mathbf{t}_i)' \boldsymbol{\beta}) + \mathbf{F}_{\mathbf{t}_i}^{-1} \mathbf{B}_{\mathbf{t}_i} \mathbf{w}_{N(\mathbf{t}_i)}$. Finally, we update the components of \mathbf{w}_S individually. For any two locations \mathbf{s} and \mathbf{t} in \mathcal{D} , if $\mathbf{s} \in N(\mathbf{t})$ and is the l -th component of $N(\mathbf{t})$, i.e., say $\mathbf{s} = N(\mathbf{t})(l)$, then define $\mathbf{B}_{\mathbf{t}, \mathbf{s}}$ as the $l \times l$ submatrix formed by columns $(l-1)q+1, (l-1)q+2, \dots, lq$ of $\mathbf{B}_{\mathbf{t}}$. Let $U(\mathbf{s}_i) = \{\mathbf{t} \in \mathcal{S} \cup \mathcal{T} | \mathbf{s}_i \in N(\mathbf{t})\}$ and for every $\mathbf{t} \in U(\mathbf{s}_i)$ define, $\mathbf{a}_{\mathbf{t}, \mathbf{s}_i} = \mathbf{w}(\mathbf{t}) - \sum_{\mathbf{s} \in N(\mathbf{t}), \mathbf{s} \neq \mathbf{s}_i} \mathbf{B}_{\mathbf{t}, \mathbf{s}} \mathbf{w}(\mathbf{s})$. Then, for $i = 1, 2, \dots, k$, we have the full conditional $\mathbf{w}_{\mathbf{s}_i} | \cdot \sim N(\mathbf{V}_{\mathbf{s}_i} \boldsymbol{\mu}_{\mathbf{s}_i}, \mathbf{V}_{\mathbf{s}_i})$ where $\mathbf{V}_{\mathbf{s}_i} = (In(\mathbf{s}_i \in \mathcal{S}^*) \mathbf{Z}(\mathbf{s}_i) \mathbf{D}^{-1} \mathbf{Z}(\mathbf{s}_i)' + \mathbf{F}_{\mathbf{s}_i}^{-1} + \sum_{\mathbf{t} \in U(\mathbf{s}_i)} \mathbf{B}'_{\mathbf{t}, \mathbf{s}_i} \mathbf{F}_{\mathbf{t}}^{-1} \mathbf{B}_{\mathbf{t}, \mathbf{s}_i})^{-1}$, $\boldsymbol{\mu}_{\mathbf{s}_i} = In(\mathbf{s}_i \in \mathcal{S}^*) \mathbf{Z}(\mathbf{s}_i) \mathbf{D}^{-1} (\mathbf{y}(\mathbf{s}_i) - \mathbf{X}(\mathbf{s}_i)' \boldsymbol{\beta}) + \mathbf{F}_{\mathbf{s}_i}^{-1} \mathbf{B}_{\mathbf{s}_i} \mathbf{w}_{N(\mathbf{s}_i)} + \sum_{\mathbf{t} \in U(\mathbf{s}_i)} \mathbf{B}'_{\mathbf{t}, \mathbf{s}_i} \mathbf{F}_{\mathbf{t}}^{-1} \mathbf{a}_{\mathbf{t}, \mathbf{s}_i}$ and $In(\cdot)$ denotes the indicator function. Hence, the \mathbf{w} 's can also be updated without requiring storage or factorization of any $n \times n$ matrices.

Turning to predictions, let \mathbf{t} be a new location where we intend to predict $\mathbf{y}(\mathbf{t})$ given $\mathbf{X}(\mathbf{t})$ and $\mathbf{Z}(\mathbf{t})$. The Gibbs sampler for estimation also generates the posterior samples $\mathbf{w}_S | \mathbf{y}$. So, if $\mathbf{t} \in \mathcal{S}$, then we simply get samples of $\mathbf{y}(\mathbf{t}) | \mathbf{y}$ from $N(\mathbf{X}(\mathbf{t})' \boldsymbol{\beta} + \mathbf{Z}(\mathbf{t})' \mathbf{w}(\mathbf{t}), \mathbf{D})$.

If \mathbf{t} is outside \mathcal{S} , then we generate samples of $\mathbf{w}(\mathbf{t})$ from its full conditional, $N(\mathbf{V}_t\boldsymbol{\mu}_t, \mathbf{V}_t)$, where $\mathbf{V}_t = (\mathbf{Z}(\mathbf{t})\mathbf{D}^{-1}\mathbf{Z}(\mathbf{t})' + \mathbf{F}_t^{-1})^{-1}$ and $\boldsymbol{\mu}_t = \mathbf{Z}(\mathbf{t})\mathbf{D}^{-1}(\mathbf{y}(\mathbf{t}) - \mathbf{X}(\mathbf{t})'\boldsymbol{\beta}) + \mathbf{F}_t^{-1}\mathbf{B}_t\mathbf{w}_{N(\mathbf{t})}$, and subsequently generate posterior samples of $\mathbf{y}(\mathbf{t}) | \mathbf{y}$ similar to the earlier case.

3.3 Computational complexity

Implementing the NNGP model in Section 3.2 reveals that one entire pass of the Gibbs sampler can be completed without any large matrix operations. The only difference between (9) and a full geostatistical hierarchical model is that the spatial process is modeled as an NNGP prior as opposed a standard GP. For comparisons, we offer rough estimates of the flop counts to generate $\boldsymbol{\theta}$ and \mathbf{w} per iteration of the sampler. For all locations, $\mathbf{t} \in \mathcal{S} \cup \mathcal{T}$, \mathbf{B}_t and \mathbf{F}_t can be calculated using $O(m^3q^3)$ flops. So, from (10) it is easy to see that $p(\boldsymbol{\theta} | \cdot)$ can be calculated using $O((n - r + k)m^3q^3)$ flops. For locations in \mathcal{U} , calculating the terms $\boldsymbol{\mu}_{t_i}$ and \mathbf{V}_{t_i} requires a total of $O((n - r)l^2q^2)$ additional flops. For the locations in \mathcal{S} , if \mathbf{s}_i is in the neighbor set of, say, n_i number of locations in $\mathcal{S} \cup \mathcal{T}$ then we can compute $\mathbf{V}_{\mathbf{s}_i}$ and $\boldsymbol{\mu}_{\mathbf{s}_i}$ in $O(n_i(mq^3 + q^2l^2))$ additional flops. As $\sum_{i=1}^n n_i \leq (n - r + k)m$, it is possible to generate a set of posterior samples for \mathbf{w} and $\boldsymbol{\theta}$ using $O((n - r + k)m(m^3q^3 + q^2l^2))$ flops.

Therefore, the flop count is linear in the total number of locations in $\mathcal{S} \cup \mathcal{T}$ and ensures scalability of the NNGP to large datasets. Compare this with a full GP model with a dense correlation matrix, which requires $O(n^3q^3)$ flops for updating \mathbf{w} in each iteration. Simulation results in Section 5.1 indicate that NNGP models with usually very small values of m (≈ 10) provides inference almost indistinguishable to full geostatistical models. Therefore, for large n , this linear flop count is drastically less. Also, linearity with respect to k ensures a feasible implementation even for $k \approx n$. This offers substantial improvement over low rank models where the computational cost is quadratic in the number of “knots,” which must kept small thereby resulting in oversmoothing. Also, both the full geostatistical and the predictive process models require storage of the $n \times n$ distance matrix, which can potentially exhaust storage resources for large datasets. An NNGP model only requires the distance matrix between neighbors for every location, thereby storing $n - r + k$ small matrices, each of order $m \times m$. Hence, NNGP accrues substantial computational benefits over existing methods for very large spatial datasets and may be the only feasible option for fully model-based inference in certain cases, as seen in the forestry data example (Section 5).

3.4 Choice of \mathcal{S} , neighbors and m

As elaborated in Section 2, given any parent Gaussian process and *any* fixed reference set of locations \mathcal{S} , we can construct a valid nearest-neighbor spatial process. The resulting distributions for the realizations of the NNGP depend upon the choice of the reference set \mathcal{S} , the choice of $N(\mathbf{s}_i)$'s and the size of each $N(\mathbf{s}_i)$, i.e., m . Unlike the number of “knots” in low rank models, the number of points in \mathcal{S} do not thwart computational scalability. From Section 3.3, we observe that the flop count in an NNGP model only increases linearly with the size of \mathcal{S} . Hence, the number of locations in \mathcal{S} can, in theory, be large and this provides a lot of flexibility in choosing \mathcal{S} .

Points over a grid across the entire domain seem to be a plausible choice for \mathcal{S} . For example, we can construct a large \mathcal{S} using a dense grid to improve performance without adversely affecting computational costs. Another, perhaps even simpler, option for large datasets is to simply fix $\mathcal{S} = \mathcal{T}$, the set of observed locations. Since the NNGP is a legitimate process for any fixed \mathcal{S} , this choice is legitimate and it reduces computational costs even further by avoiding additional sampling of $\mathbf{w}_{\mathcal{U}}$ in the Gibbs sampler. Our empirical investigations (see Section 5.1) reveal that choosing $\mathcal{S} = \mathcal{T}$ deliver inference almost indistinguishable from choosing \mathcal{S} to be a grid over the domain for large datasets.

For our subsequent analysis, we have constructed the neighbor sets for \mathcal{S} based on (2). Stein et al. (2004) explored several other design schemes for selecting neighbor sets. He proposed the use of a sandwich variance estimator for evaluating all such competing designs but conceded accrual of additional computational costs and that this approach may not be ideal in spatial settings with irregularly placed data points. The asymptotic properties of the composite likelihood estimators derived in Eidsvik et al. (2014) suffers from the same limitations. In Section 2 we proved that all conforming choices for $N(\mathbf{s})$ (including, for example, those stipulated in Stein et al. (2004)) yield valid NNGP models. Therefore, for any given dataset, all these candidate schemes for choosing neighbor sets can be easily compared using any standard model comparison metrics such as DIC (Spiegelhalter et al. 2002), GPD (Gelfand and Ghosh 1998) or RMSPE(RMSECV) (Yeniay and Goktas 2002) and the best scheme can be chosen accordingly. The same model comparison metrics are also used to compare NNGP models to full geostatistical or predictive process models and also for selecting the size of the neighbor sets m . However, as we illustrate later in Section 5.1 usually a small value of m between 10 to 15 produces performance at par with the full geostatistical model. While larger m may be beneficial for massive datasets, perhaps under a different design scheme, it is still going to be much smaller than the number of knots required in low rank models (see Section 5.1). The implementation algorithm outlined in Section 3 remains the same for any of these conforming choices of \mathcal{S} , $N(\mathbf{s}_i)$'s and m , providing additional flexibility of design for NNGP models. Section 5 provides details of model assessment for various scenarios using simulated and real datasets.

4 Alternate NNGP models and algorithms

Consider observations measured at a large number of fixed spatial locations and suppose we fix the reference set \mathcal{S} to be the set of observed spatial locations. The Gibbs sampling algorithm detailed in Section 3.2 is extremely efficient for large datasets due to linear flop count. An alternative to sequential updating is to perform block updates of $\mathbf{w}_{\mathcal{S}}$. Since $\mathcal{S} = \mathcal{T}$, $\mathbf{s}_i = \mathbf{t}_i$ for all $i = 1, 2, \dots, n$ and so we denote $\mathbf{w}_{\mathcal{S}} = \mathbf{w}_{\mathcal{T}}$ by \mathbf{w} . Then,

$$\mathbf{w}|\cdot \sim N(\mathbf{V}_{\mathcal{S}}\mathbf{Z}'\mathbf{D}_n^{-1}(\mathbf{y} - \mathbf{X}\boldsymbol{\beta}), \mathbf{V}_{\mathcal{S}}), \quad \text{where } \mathbf{V}_{\mathcal{S}} = (\mathbf{Z}'\mathbf{D}_n^{-1}\mathbf{Z} + \tilde{\mathbf{C}}_{\mathcal{S}}^{-1})^{-1}. \quad (11)$$

Recall that $\tilde{\mathbf{C}}_{\mathcal{S}}^{-1}$ is sparse (Theorem 2). Since \mathbf{Z} and \mathbf{D}_n are block diagonal, $\mathbf{V}_{\mathcal{S}}^{-1}$ retains the sparsity of $\tilde{\mathbf{C}}_{\mathcal{S}}^{-1}$. So, a sparse Cholesky factorization of $\mathbf{V}_{\mathcal{S}}^{-1}$ will efficiently produce the Cholesky factors of $\mathbf{V}_{\mathcal{S}}$. This will facilitate block updating of \mathbf{w} in the Gibbs sampler.

Another possible approach involves NNGP models for the response $\mathbf{y}(\mathbf{s})$. If $\mathbf{w}(\mathbf{s})$ is a Gaussian Process, then so is $\mathbf{y}(\mathbf{s}) = \mathbf{Z}(\mathbf{s})'\mathbf{w}(\mathbf{s}) + \epsilon$ (without loss of generality we assume $\beta = \mathbf{0}$). One can directly use the NNGP specification for $\mathbf{y}(\mathbf{s})$ instead of $\mathbf{w}(\mathbf{s})$. That is, we derive $\mathbf{y}(\mathbf{s}) \sim NNGP(\mathbf{0}, \tilde{\Sigma}(\cdot, \cdot))$ from the parent Gaussian process $GP(\mathbf{0}, \Sigma(\cdot, \cdot | \boldsymbol{\theta}))$. The Gibbs sampler analogous to Section 3 now enjoys the additional advantage of avoiding full conditionals for \mathbf{w} . This results in a Bayesian analogue for Vecchia (1988) and Stein et al. (2004). However, this precludes inference on the spatial residual surface $\mathbf{w}(\mathbf{s})$. Inferring on \mathbf{w} 's provides additional insight into understanding the spatial contours of the residual surface and is often important in identifying lurking covariates and eliciting unexplained spatial patterns. Vecchia (1992) used the nearest neighbor approximation on a spatial model for observations (\mathbf{y}) with independent measurement error (nuggets) in addition to the usual spatial component (\mathbf{w}). However, it may not be possible to recover \mathbf{w} using this approach. For example, a univariate stationary process $\mathbf{y}(\mathbf{s})$ with a nugget effect can be decomposed as $\mathbf{y}(\mathbf{s}) = \mathbf{w}(\mathbf{s}) + \epsilon(\mathbf{s})$ (letting $\beta = \mathbf{0}$) for some $\mathbf{w}(\mathbf{s}) \sim GP(\mathbf{0}, \mathbf{C}(\cdot, \cdot | \boldsymbol{\theta}))$ and white noise process $\epsilon(\mathbf{s})$. If $\mathbf{y} = \mathbf{w} + \epsilon$, where $\mathbf{w} \sim N(\mathbf{0}, \mathbf{C})$, $\epsilon \sim N(\mathbf{0}, \tau^2 \mathbf{I}_n)$, then $\text{Cov}(\mathbf{y}) = \mathbf{C} + \tau^2 \epsilon = \Sigma$, all eigenvalues of Σ are greater than τ^2 and $\text{Cov}(\mathbf{w} | \mathbf{y}) = \tau^2 \mathbf{I}_n - \tau^4 \Sigma^{-1}$. For the nearest neighbor approximations, however, the eigenvalues of $\tilde{\Sigma}$ need not be greater than τ^2 , so the above covariance matrix need not be positive definite on the entire support of τ^2 .

A variant of the above model is obtained by using a NNGP prior for \mathbf{w} , as in (9), and then integrating out \mathbf{w} . The resulting likelihood is $N(\mathbf{y} | \mathbf{X}\beta, \Sigma_y)$, where $\Sigma_y = \mathbf{Z}\tilde{\mathbf{C}}_S\mathbf{Z}' + \mathbf{D}_n$ and the Bayesian specification is completed using priors on β , τ_j^2 's and $\boldsymbol{\theta}$ as in (9). This model drastically reduces the number of variables in the Gibbs sampler, while preserving the nugget effect in the parent model. Posterior inference on \mathbf{w} now proceeds by sampling from $p(\mathbf{w} | \mathbf{y}) = \int p(\mathbf{w} | \boldsymbol{\theta}, \beta, \{\tau_j^2\}, \mathbf{y})p(\boldsymbol{\theta}, \beta, \{\tau_j^2\} | \mathbf{y})$ using composition sampling—we draw $\mathbf{w}^{(g)}$ from $p(\mathbf{w} | \boldsymbol{\theta}^{(g)}, \beta^{(g)}, \{\tau_j^{2(g)}\}, \mathbf{y})$ one-for-one for each sampled parameter.

With the same prior specifications as in (9), we can generate the full conditionals for the parameters in the marginalized model as follows: $\beta | \mathbf{y}, \phi \sim N((\mathbf{V}_\beta^{-1} + \mathbf{X}'\Sigma_y^{-1}\mathbf{X})^{-1}(\mathbf{V}_\beta^{-1}\boldsymbol{\mu}_\beta + \mathbf{X}'\Sigma_y^{-1}\mathbf{y}), (\mathbf{V}_\beta^{-1} + \mathbf{X}'\Sigma_y^{-1}\mathbf{X})^{-1})$. It is difficult to factor out τ_j^2 's from Σ_y^{-1} , so conjugacy is lost with respect to any standard prior. Metropolis block updates for $\boldsymbol{\theta}$ are feasible for any tractable prior $p(\boldsymbol{\theta})$. We compute $\mathbf{X}'\Sigma_y^{-1}\mathbf{X}$, $\mathbf{X}'\Sigma_y^{-1}\mathbf{y}$ and $(\mathbf{y} - \mathbf{X}\beta)'\Sigma_y^{-1}(\mathbf{y} - \mathbf{X}\beta)$. Since $\Sigma_y^{-1} = \mathbf{D}_n^{-1} - \mathbf{D}_n^{-1}\mathbf{Z}(\tilde{\mathbf{C}}_S^{-1} + \mathbf{Z}'\mathbf{D}_n^{-1}\mathbf{Z})^{-1}\mathbf{Z}'\mathbf{D}_n^{-1} = \mathbf{D}_n^{-1} - \mathbf{D}_n^{-1}\mathbf{Z}\mathbf{V}_S\mathbf{Z}'\mathbf{D}_n^{-1}$, where \mathbf{V}_S is given by (11), a sparse Cholesky factorization of \mathbf{V}_S^{-1} imparts efficiency.

Using block update for \mathbf{w}_S in (9) and fitting the marginalized version of (9) both require an efficient sparse Cholesky solver for \mathbf{V}_S^{-1} . There is a growing literature on sparse symmetric solvers (Davis 2006). Note that computational expenses for most sparse Cholesky algorithms depend on the precise nature of the sparse structure (mostly on the bandwidth) of $\tilde{\mathbf{C}}_S^{-1}$. Figure 2 suggests this may vary significantly based on construction and size of neighborhood sets. Therefore, the total number of flops required for Gibbs sampling and prediction in this marginalized model can vary on the sparse nature of $\tilde{\mathbf{C}}_S^{-1}$ and it may, sometimes, heavily exceed the linear usage achieved by the unmarginalized model with individual updates for \mathbf{w}_i . Therefore, it may be prudent to choose the precise fitting algorithms based on the sparsity structure of the matrix $\tilde{\mathbf{C}}_S^{-1}$ for the given dataset.

5 Illustrations

We conduct simulation experiments and analyze a large forestry dataset to assess model performance with regard to learning about process parameters and predicting at new locations. Posterior inference for subsequent analysis were based upon three chains of 25000 iterations (with a burn-in of 5000 iterations). The samplers were programmed in C++ and leveraged Intel's Math Kernel Library's (MKL) threaded BLAS and LAPACK routines for matrix computations. The computations were conducted on a Linux workstation using two Intel Nehalem quad-Xeon processors.

5.1 Simulation experiments

We generated observations using 2500 locations within a unit square domain from the model (8) with $q = l = 1$ (univariate outcome), $p = 2$, $\mathbf{Z}(\mathbf{t})' = 1$ (scalar), the spatial covariance matrix $\mathbf{C}(\boldsymbol{\theta}) = \sigma^2 \mathbf{R}(\boldsymbol{\phi})$, where $\mathbf{R}(\boldsymbol{\phi})$ is a $n \times n$ correlation matrix, and $\mathbf{D} = \tau^2$ (scalar). The model included an intercept and a covariate \mathbf{x}_1 drawn from $N(0, 1)$. The (i, j) th element of $\mathbf{R}(\boldsymbol{\phi})$ was calculated using the Matérn function

$$\rho(\mathbf{t}_i, \mathbf{t}_j; \boldsymbol{\phi}) = \frac{1}{2^{\nu-1} \Gamma(\nu)} (\|\mathbf{t}_i - \mathbf{t}_j\| \phi)^\nu \mathcal{K}_\nu(\|\mathbf{t}_i - \mathbf{t}_j\| \phi); \phi > 0, \nu > 0, \quad (12)$$

where $\|\mathbf{t}_i - \mathbf{t}_j\|$ is the Euclidean distance between locations \mathbf{t}_i and \mathbf{t}_j , $\boldsymbol{\phi} = (\phi, \nu)$ with ϕ controlling the decay in spatial correlation and ν controlling the process smoothness, Γ is the usual Gamma function while \mathcal{K}_ν is a modified Bessel function of the second kind with order ν (Stein 1999). Evaluating the Gamma function for each matrix element within each iteration requires substantial computing time and can obscure differences in sampler run times; hence, we fixed ν at 0.5 which reduces (12) to the exponential correlation function. The first column in Table 1 gives the *true* values used to generate the responses. Figure 4(a) illustrates the $w(\mathbf{t})$ surface interpolated over the domain.

We then estimated the following models from the full data: *i*) the full Gaussian Process (*Full GP*); *ii*) the NNGP with $m = \{1, 2, \dots, 25\}$ for $\mathcal{S} \neq \mathcal{T}$ and $\mathcal{S} = \mathcal{T}$, and; *iii*) a Gaussian Predictive Process (GPP) model (Banerjee et al. 2008) with 64 knots placed on a grid over the domain. For the NNGP with $\mathcal{S} \neq \mathcal{T}$ we considered 2000 randomly placed reference locations within the domain. The 64 knot GPP was chosen because its computing time was comparable to that of NNGP models. We used an efficient marginalized sampling algorithm for the Full GP and GPP models as implemented in the `spBayes` package in R (Finley et al. 2013). We fit all the models to 2000 of the 2500 observed locations, while the remaining 500 observations were withheld to assess the model's predictive performance.

For all models, the intercept and slope regression parameters, β_0 and β_1 , were given *flat* prior distributions. The variance components σ^2 and τ^2 were assigned inverse-Gamma $IG(2, 1)$ and $IG(2, 0.1)$ priors, respectively, and the spatial decay ϕ received a uniform prior $U(3, 30)$. The prior distributions on ϕ corresponds to support between approximately 0.1 and 1 domain distance units.

Parameter estimates and performance metrics for the NNGP (with $m = 10$ and $m = 20$),

Table 1: Univariate synthetic data analysis parameter estimates and computing time in minutes for NNGP and full GP models. Parameter posterior summary 50 (2.5, 97.5) percentiles.

	True	NNGP ($\mathcal{S} \neq \mathcal{T}$)		NNGP ($\mathcal{S} = \mathcal{T}$)	
		$m = 10, k = 2000$	$m = 20, k = 2000$	$m = 10$	$m = 20$
β_0	1	0.99 (0.71, 1.48)	1.02 (0.73, 1.49)	1.00 (0.62, 1.31)	1.03 (0.65, 1.34)
β_1	5	5.00 (4.98, 5.03)	5.01 (4.98, 5.03)	5.01 (4.99, 5.03)	5.01 (4.99, 5.03)
σ^2	1	1.09 (0.89, 1.49)	1.04 (0.85, 1.40)	0.96 (0.78, 1.23)	0.94 (0.77, 1.20)
τ^2	0.1	0.07 (0.04, 0.10)	0.07 (0.04, 0.10)	0.10 (0.08, 0.13)	0.10 (0.08, 0.13)
ϕ	12	11.81 (8.18, 15.02)	12.21 (8.83, 15.62)	12.93 (9.70, 16.77)	13.36 (9.99, 17.15)
PD	-	1491.08	1478.61	1243.32	1249.57
DIC	-	1856.85	1901.57	2390.65	2377.51
G	-	33.67	35.68	77.84	76.40
P	-	253.03	259.13	340.40	337.88
D	-	286.70	294.82	418.24	414.28
GRS	-	3870.16	3813.11	3083.47	3103.23
RMSPE	-	1.22	1.22	1.2	1.2
95% CI cover %	-	97.2	97.2	97.6	97.6
95% CI width	-	2.19	2.18	2.13	2.12
Time	-	20.29	65.31	14.40	46.47

	True	Predictive Process	Full
		64 knots	Gaussian Process
β_0	1	1.30 (0.54, 2.03)	1.03 (0.69, 1.34)
β_1	5	5.03 (4.99, 5.06)	5.01 (4.99, 5.03)
σ^2	1	1.29 (0.96, 2.00)	0.94 (0.76, 1.23)
τ^2	0.1	0.08 (0.04, 0.13)	0.10 (0.08, 0.12)
ϕ	12	5.61 (3.48, 8.09)	13.52 (9.92, 17.50)
PD	-	1258.27	1260.68
DIC	-	13677.97	2364.80
G	-	1075.63	74.80
P	-	200.39	333.27
D	-	1276.03	408.08
GRS	-	-6267.66	3134.47
RMSPE	-	1.68	1.2
95% CI cover %	-	95.6	97.6
95% CI width	-	2.97	2.12
Time	-	43.36	560.31

GPP, and the Full GP models are provided in Table 1. All model specifications produce similar posterior median and 95% credible intervals estimates, with the exception of ϕ in the 64 knot GPP model. Larger values of DIC and D suggest that the GPP model does not fit the data as well as the NNGP and Full GP models. The NNGP $\mathcal{S} = \mathcal{T}$ models provide DIC, D, and GRS scores that are comparable to those of the Full GP model. These fit metrics suggest the NNGP $\mathcal{S} \neq \mathcal{T}$ models provide better fit to the data than that achieved by the full GP model which is probably due to overfitting caused by a very large reference set \mathcal{S} . The last row in Table 1 shows computing times in minutes for one chain of 25000 iterations reflecting on the enormous computational gains of NNGP models over full GP model.

Turning to the out-of-sample prediction results. The Full model's RMSPE and mean width between the upper and lower 95% posterior predictive credible interval is 1.2 and 2.12, respectively. As shown in Figure 3, comparable RMSPE and mean interval width for the NNGP $\mathcal{S} = \mathcal{T}$ model is achieved by $m \approx 10$. There was negligible difference between the predictive performance of the NNGP $\mathcal{S} \neq \mathcal{T}$ and $\mathcal{S} = \mathcal{T}$ models. Both the NNGP and Full GP model have better predictive performance than the Predictive Process models when the number of knots is small, e.g., 64. All models showed appropriate 95% credible interval coverage rates.

Figures 4(b-f) illustrate the posterior median estimates of the spatial random effects from the Full GP, NNGP ($\mathcal{S} = \mathcal{T}$) with $m = 10$ and $m = 20$, NNGP ($\mathcal{S} \neq \mathcal{T}$) with $m = 10$ and GPP models. These surfaces can be compared to the *true* surface depicted in Figure 4(a). This comparison shows: *i*) the NNGP models closely approximates the true surface and that estimated by the Full GP model, and; *ii*) the reduced rank predictive process model based

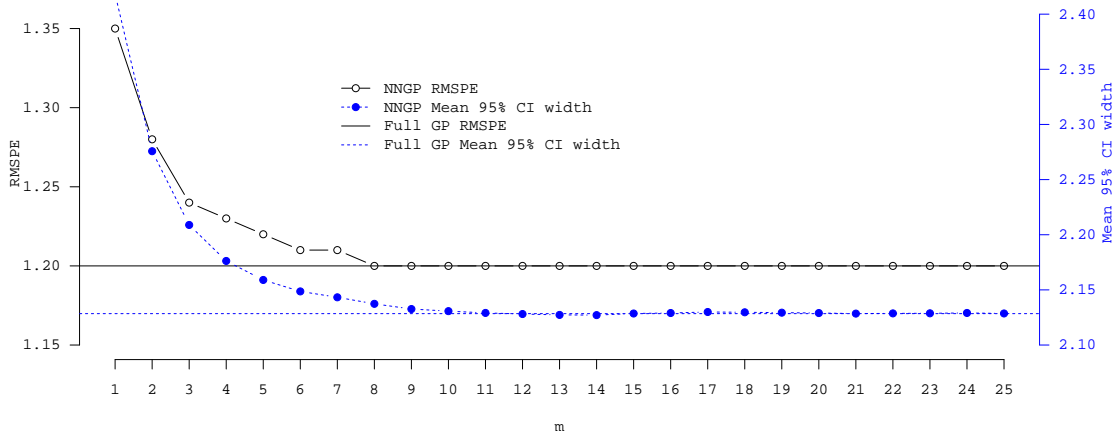


Figure 3: Choice of m in NNGP models: Out-of-sample Root Mean Squared Prediction Error (RMSPE) and mean width between the upper and lower 95% posterior predictive credible intervals for a range of m for the univariate synthetic data analysis

on 64 knots greatly smooths over small-scale patterns. This last observation highlights one of the major criticisms of reduced rank models Stein (2013) and illustrates why these models often provide compromised predictive performance when the true surface has fine spatial resolution details. Overall, we see the clear computational advantage of the NNGP over the Full GP model, and both inferential and computational advantage over the GPP model.

5.2 Forest biomass data analysis

Information about the spatial distribution of forest biomass is needed to support global, regional, and local scale decisions, including assessment of current carbon stock and flux, bio-feedstock for emerging bio-economies, and impact of deforestation. In the United States, the Forest Inventory and Analysis (FIA) program of the USDA Forest Service collects the data needed to support these assessments. The program has established field plot centers in permanent locations using a sampling design that produces an equal probability sample (Bechtold and Patterson 2005). Field crews recorded stem measurements for all trees with diameter at breast height (DBH); 1.37 m above the forest floor) of 12.7 cm or greater. Given these data, established allometric equations were used to estimate each plot’s forest biomass. For the subsequent analysis, plot biomass was scaled to metric tons per ha then square root transformed. The transformation ensures that back transformation of subsequent predicted values have support greater than zero and helps to meet basic regression models assumptions.

Figure 5(a) illustrates the georeferenced forest inventory data consisting of 114,371 forested FIA plots measured between 1999 and 2006 across the conterminous United States. The two blocks of missing observations in the Western and Southwestern United States correspond to Wyoming and New Mexico, which have not yet released FIA data. Figure 5(b) shows a deterministic interpolation of forest biomass observed on the FIA plots. Dark blue

indicates high forest biomass, which is primarily seen in the Pacific Northwest, Western Coastal ranges, Eastern Appalachian Mountains, and in portions of New England. In contrast, dark red indicates regions where climate or land use limit vegetation growth.

A July 2006 Normalized Difference Vegetation Index (NDVI) image from the MODerate-resolution Imaging Spectroradiometer (MODIS); <http://g1cf.umd.edu/data/ndvi>) sensor was used as a single predictor. NDVI is calculated from the visible and near-infrared light reflected by vegetation, and can be viewed as a measure of greenness. In this image, Figure 5(c), dark green corresponds to dense vegetation whereas brown identifies regions of sparse or no vegetation, e.g., in the Southwest. NDVI is commonly used as a covariate in forest biomass regression models, see, for e.g., Zhang and Kondraguanta (2006). Results from these and similar studies show a positive linear relationship between forest biomass and NDVI. The strength of this relationship, however, varies by forest tree species composition, age, canopy structure, and level of reflectance. We expect a space-varying relationship between biomass and NDVI, given tree species composition and disturbance regimes generally exhibit strong spatial dependence across forested landscapes.

The ~ 38 gigabytes of memory in our workstation was insufficient for storage of distance matrices required to fit a Full GP or GPP model. In the subsequent analysis we explore the relationship between forest biomass and NDVI using a non-spatial model, a NNGP space-varying intercept (SVI) model (i.e., $q = l = 1$ and $\mathbf{Z}(\mathbf{t}) = 1$) in (8), and a NNGP spatially-varying coefficients (SVC) regression model with $l = 1$, $q = p = 2$ and $\mathbf{Z}(\mathbf{t}) = \mathbf{X}(\mathbf{t})$ in (8). The reference sets for the NNGP models were again the observed locations and $m = 5$. The parent process $\mathbf{w}(\mathbf{t})$ is a bivariate Gaussian process with a stationary cross-covariance specification $\mathbf{C}(\mathbf{t}_i, \mathbf{t}_j | \boldsymbol{\theta}) = \mathbf{A}\boldsymbol{\Gamma}(\boldsymbol{\phi})\mathbf{A}'$, where \mathbf{A} is 2×2 lower-triangular with positive diagonal elements, $\boldsymbol{\Gamma}$ is 2×2 diagonal with $\rho(\mathbf{t}_i, \mathbf{t}_j; \boldsymbol{\phi}_b)$ (defined in (12)) as the b^{th} diagonal entry, $b = 1, 2$ and $\boldsymbol{\phi}_b = (\phi_b, \nu_b)'$ (see, e.g., Gelfand and Banerjee 2010).

For all models, the intercept and slope regression parameters were given *flat* prior distributions. The variance components τ^2 and σ^2 were assigned inverse-Gamma $IG(2, 1)$ priors, the SVC model cross-covariance matrix $\mathbf{A}\mathbf{A}'$ followed an inverse-Wishart $IW(3, 0.1)$, and the Matérn spatial decay and smoothness parameters received uniform prior supports $U(0.01, 3)$ and $U(0.1, 2)$, respectively. These prior distributions on ϕ and ν correspond to support between approximately 0.5 and 537 km. Candidate models are assessed using the goodness of fit metrics referenced in Section 3.4, inference drawn from mapped estimates of the regression coefficients, and out-of-sample prediction.

Candidate models are assessed using the goodness of fit metrics referenced in Section 3.4 and inference drawn from mapped estimates of the regression coefficients. Model parameter estimates and performance metrics are given in Table 2. Relative to the spatial models, the non-spatial model has higher values of DIC and D which suggests NDVI alone does not adequately capture the spatial structure of forest biomass. This observation is corroborated using a variogram fit to the non-spatial model’s residuals, Figure 5(d). The variogram shows a nugget of ~ 0.42 , partial sill of ~ 0.05 , and range of ~ 150 km. This residual spatial dependence is apparent when we map the SVI model spatial random effects as shown in Figure 5(e). This map, and the estimate of a non-negligible spatial variance σ^2 in Table 2, suggests the addition of a spatial random effect was warranted and helps satisfy the model

Table 2: Forest biomass data analysis parameter estimates and computing time in hours for candidate models. Parameter posterior summary 50 (2.5, 97.5) percentiles.

	NNGP		NNGP
	Non-spatial	Space-varying intercept	Space-varying coefficients
β_0	1.043 (1.02, 1.065)	1.44 (1.39, 1.48)	1.23 (1.20, 1.26)
β_{NDVI}	0.0093 (0.009, 0.0095)	0.0061 (0.0059, 0.0062)	0.0072 (0.0071, 0.0074)
σ^2	–	0.16 (0.15, 0.17)	–
$\mathbf{A}\mathbf{A}'_{1,1}$	–	–	0.24 (0.23, 0.24)
$\mathbf{A}\mathbf{A}'_{2,1}$	–	–	-0.00088 (-0.00093, -0.00083)
$\mathbf{A}\mathbf{A}'_{2,2}$	–	–	0.0000052 (0.0000047, 0.0000056)
τ^2	0.52 (0.51, 0.52)	0.39 (0.39, 0.40)	0.39 (0.38, 0.40)
ϕ_1	–	0.016 (0.015, 0.016)	0.022 (0.021, 0.023)
ϕ_2	–	–	0.030 (0.029, 0.031)
ν_1	–	0.66 (0.64, 0.67)	0.92 (0.90, 0.93)
ν_2	–	–	0.92 (0.89, 0.93)
p_D	2.94	6526.95	4976.13
DIC	250137	224484.2	222845.1
G	59765.30	42551.08	43117.37
P	59667.15	47603.47	46946.49
D	119432.45	90154.55	90063.86
Time	–	16.36	45.74

assumption of uncorrelated residuals.

The values of the SVC model’s goodness of fit metrics suggest that allowing the NDVI regression coefficient to vary spatially improves model fit over that achieved by the SVI model. Figures 6(a) and 6(b) show maps of the SVC model coefficient estimates for the intercept and NDVI, respectively. The clear regional patterns seen in Figure 6(b) suggest the relationship between NDVI and biomass does vary spatially—with stronger positive regression coefficients in the Pacific Northwest and northern California areas. Forest in the Pacific Northwest and northern California is dominated by conifers and support the greatest range in biomass per unit area within the entire conterminous United States. The other strong regional pattern seen in Figure 6(b) is across western New England, where near zero regression coefficients suggest that NDVI is not as effective at discerning differences in forest biomass. This result is not surprising. For deciduous forests NDVI can explain variability in low to moderate vegetation density. However, in high biomass deciduous forests, like those found across western New England, NDVI *saturates* and is no longer sensitive to changes in vegetation structure (Wang et al. 2005) hence we see a higher intercept value in this region but lower slope coefficient on NDVI.

Figures 6(c) and 6(d) map each location’s posterior predictive distribution median and range between the upper and lower 95% credible interval, respectively, from the SVC model. We see strong correspondence between Figure 6(c) and the non-statistical interpolation of biomass in Figure 5(b). The measure of prediction uncertainty in Figure 6(d) provides a

realistic depiction of the model’s ability to quantify forest biomass across the United States.

Candidate model prediction performance was also assessed using prediction mean squared error (PMSE). Here we fit the candidate models using 100,000 observations and withheld 14,371 for validation. PMSE for the non-spatial, SVI, and SVC models was 0.52, 0.41, and 0.42 respectively. Lower PMSE for the spatial models, versus the non-spatial model, corroborates the results from the model fit metrics and further supports the need for spatial random effects in the analysis.

6 Summary and conclusions

We have proposed a class of highly scalable hierarchical spatial models based upon a formally defined Nearest-Neighbor Gaussian process (NNGP) to carry out fully model-based inference for geostatistical datasets. We introduce no new parameters and the NNGP is constructed using a fixed reference set \mathcal{S} comprising any k locations in the spatial domain. Storage and flops are linear in k and larger values of k do not thwart computations. The reference set helps create a class of neighborhoods that will ensure a valid stochastic process so that spatial interpolation or kriging is coherent. This distinguishes the NNGP from alternate likelihood approximation approaches involving composite likelihoods. The realizations of the NNGP have valid probability densities that are not degenerate, no matter what k is.

The scalability of the NNGP (in terms of flops and storage) comes from the number of neighbors m constructed from \mathcal{S} . While some sensitivity to m and the choice of points in \mathcal{S} is expected, our results indicate that inference becomes robust rapidly and large values of m are not required. Perhaps, more importantly, the NNGP does not suffer from the inferential limitations of certain low-rank models (e.g., biases caused by oversmoothing) and delivers inference practically indistinguishable from geostatistical models.

Further explorations, both theoretical and empirical, regarding the role of \mathcal{S} , k and m will be desirable. For certain choices of \mathcal{S} , as m becomes large, the NNGP gets closer to the parent process. However, the role of k is more subtle. What happens if $k \rightarrow \infty$ when \mathcal{D} is an uncountable set of locations? Certainly the limit of the NNGP’s cross-covariance function will not tend to that of the process. It is unclear if the induced process will tend to the parent process and what, if any, potential inferential benefits exist with large k . Future applications will involve spatiotemporal settings (see, e.g., Katzfuss and Cressie 2012), where one will need to consider neighbors both in space and time to derive an NNGP. More generally, the NNGP can become an effective dimension-reducing process for Gaussian process regressions in semiparametric and nonparametric models. Further scalability is possible when full Bayesian inference is not required, whence faster posterior approximation algorithms can be devised. We plan to extensively investigate the potential of NNGP models in such settings. More immediately, we plan to migrate our lower-level C++ code to the existing `spBayes` package (Finley et al. 2013) in the R statistical environment (<http://cran.r-project.org/web/packages/spBayes>) to facilitate wider user accessibility to NNGP models.

A Appendix: Proofs of results

Proof of Theorem 1: Since \mathcal{G} is a directed acyclic graph, there exists a vertex $\mathbf{s}_{\pi(1)}$ with zero out-degree i.e. no directed edge originating from it. This means $\mathbf{s}_{\pi(1)}$ does not belong to the neighbor set of any other location in \mathcal{S} . The only term where it appears on the right hand side of (1) is $p(\mathbf{w}(\mathbf{s}_{\pi(1)} | \mathbf{w}_{N(\mathbf{s}_{\pi(1)})}))$ which integrates out to one with respect to $d\mathbf{w}(\mathbf{s}_{\pi(1)})$. We now have a new acyclic directed graph \mathcal{G}_1 obtained by removing vertex $\mathbf{s}_{\pi(1)}$ and its directed edges from \mathcal{G} . Now we can find a new vertex $\mathbf{s}_{\pi(2)}$ with zero out-degree in \mathcal{G}_1 and continue as before to get a permutation $\pi(1), \pi(2), \dots, \pi(k)$ of $1, 2, \dots, k$ such that

$$\int \prod_{i=1}^k p(\mathbf{w}(\mathbf{s}_i) | \mathbf{w}_{N(\mathbf{s}_i)}) d\mathbf{w}(\mathbf{s}_{\pi(1)}) d\mathbf{w}(\mathbf{s}_{\pi(2)}) \dots d\mathbf{w}(\mathbf{s}_{\pi(k)}) = 1$$

An easy application of Fubini's theorem now ensures that this is a proper joint density. ■

Proof of Theorem 2: If $p(\mathbf{w}_{\mathcal{S}}) = N(\mathbf{w}_{\mathcal{S}} | \mathbf{0}, \mathbf{C}_{\mathcal{S}})$, then $\mathbf{w}(\mathbf{s}_i) | \mathbf{w}_{N(\mathbf{s}_i)} \sim N(\mathbf{B}_{\mathbf{s}_i} \mathbf{w}_{N(\mathbf{s}_i)}, \mathbf{F}_{\mathbf{s}_i})$, where $\mathbf{B}_{\mathbf{s}_i}$ and $\mathbf{F}_{\mathbf{s}_i}$ are defined in (3). So, the likelihood in (1) is proportional to

$$\frac{1}{\prod_{i=1}^k \sqrt{\det(\mathbf{F}_{\mathbf{s}_i})}} \exp \left(-\frac{1}{2} \sum_{i=1}^k (\mathbf{w}(\mathbf{s}_i) - \mathbf{B}_{\mathbf{s}_i} \mathbf{w}_{N(\mathbf{s}_i)})' \mathbf{F}_{\mathbf{s}_i}^{-1} (\mathbf{w}(\mathbf{s}_i) - \mathbf{B}_{\mathbf{s}_i} \mathbf{w}_{N(\mathbf{s}_i)}) \right)$$

For any matrix \mathbf{A} , let $\mathbf{A}[j : j']$ denote the submatrix formed using columns j to j' where $j < j'$. For $j = 1, 2, \dots, k$, we define $q \times q$ blocks $\mathbf{B}_{\mathbf{s}_i, j}$ as

$$\mathbf{B}_{\mathbf{s}_i, j} = \begin{cases} \mathbf{I}_q & \text{if } j = i; \\ -\mathbf{B}_{\mathbf{s}_i, l}[(l-1)q + 1 : lq] & \text{if } \mathbf{s}_j = N(\mathbf{s}_i)(l) \text{ for some } l; \\ \mathbf{0} & \text{otherwise,} \end{cases}$$

where, for any location \mathbf{s} , $N(\mathbf{s})(l)$ is the l -th neighbor of \mathbf{s} . So, $\mathbf{w}_{\mathbf{s}_i} - \mathbf{B}_{\mathbf{s}_i} \mathbf{w}_{N(\mathbf{s}_i)} = \mathbf{B}_{\mathbf{s}_i}^* \mathbf{w}_{\mathcal{S}}$, where $\mathbf{B}_{\mathbf{s}_i}^* = [\mathbf{B}_{\mathbf{s}_i, 1}, \mathbf{B}_{\mathbf{s}_i, 2}, \dots, \mathbf{B}_{\mathbf{s}_i, k}]$ is $q \times kq$ and sparse with at most $m + 1$ non-zero blocks. Then,

$$\sum_{i=1}^k (\mathbf{w}(\mathbf{s}_i) - \mathbf{B}_{\mathbf{s}_i} \mathbf{w}_{N(\mathbf{s}_i)})' \mathbf{F}_{\mathbf{s}_i}^{-1} (\mathbf{w}(\mathbf{s}_i) - \mathbf{B}_{\mathbf{s}_i} \mathbf{w}_{N(\mathbf{s}_i)}) = \sum_{i=1}^k \mathbf{w}'_{\mathcal{S}} (\mathbf{B}_{\mathbf{s}_i}^*)' \mathbf{F}_{\mathbf{s}_i}^{-1} \mathbf{B}_{\mathbf{s}_i}^* \mathbf{w}_{\mathcal{S}} = \mathbf{w}'_{\mathcal{S}} \mathbf{B}'_{\mathcal{S}} \mathbf{F}_{\mathcal{S}}^{-1} \mathbf{B}_{\mathcal{S}} \mathbf{w}_{\mathcal{S}},$$

where $\mathbf{F} = \text{diag}(\mathbf{F}_{\mathbf{s}_1}, \mathbf{F}_{\mathbf{s}_2}, \dots, \mathbf{F}_{\mathbf{s}_k})$ and $\mathbf{B}_{\mathcal{S}} = ((\mathbf{B}_{\mathbf{s}_1}^*)', (\mathbf{B}_{\mathbf{s}_2}^*)', \dots, (\mathbf{B}_{\mathbf{s}_k}^*)')'$. From the form of $\mathbf{B}_{\mathbf{s}_i, j}$, it is clear that $\mathbf{B}_{\mathcal{S}}$ is sparse and lower triangular with ones on the diagonals. So, $\det(\mathbf{B}_{\mathcal{S}}) = 1$, $\det((\mathbf{B}'_{\mathcal{S}} \mathbf{F}_{\mathcal{S}}^{-1} \mathbf{B}_{\mathcal{S}})^{-1}) = \prod \det(\mathbf{F}_{\mathbf{s}_i})$ and (1) simplifies to $N(\mathbf{w}_{\mathcal{S}} | \mathbf{0}, \tilde{\mathbf{C}}_{\mathcal{S}})$. This proves part (a).

To prove part (b), let $\tilde{\mathbf{C}}_{\mathcal{S}}^{ij}$ denote the (i, j) th block of $\tilde{\mathbf{C}}_{\mathcal{S}}^{-1}$. Then from Theorem 2 part(a) we see that for $i < j$, $\tilde{\mathbf{C}}_{\mathcal{S}}^{ij} = \sum_{l=j}^k (\mathbf{B}_{\mathbf{s}_l, i}^*)' \mathbf{F}_{\mathbf{s}_l}^{-1} \mathbf{B}_{\mathbf{s}_l, j}^*$. So, $\tilde{\mathbf{C}}_{\mathcal{S}}^{ij}$ is non-zero only if there exists at least one location \mathbf{s}_l such that $\mathbf{s}_i \in N(\mathbf{s}_l)$ and \mathbf{s}_j is either equal to \mathbf{s}_l or is in $N(\mathbf{s}_l)$. Since every neighbor set has at most m elements, there are at most $km(m+1)/2$ such pairs (i, j) . This proves part (b). ■

Proof of Theorem 3 We begin by showing that for any finite set \mathcal{V} , the expression given in

(5) is a proper density. Let $\mathcal{U} = \mathcal{V} \setminus \mathcal{S}$. Since $\mathcal{V} \cup (\mathcal{S} \setminus \mathcal{V}) = \mathcal{S} \cup \mathcal{U}$, we obtain

$$\begin{aligned} \int \tilde{p}(\mathbf{w}_{\mathcal{V}}) \prod_{\mathbf{v}_i \in \mathcal{V}} d(\mathbf{w}(\mathbf{v}_i)) &= \int \tilde{p}(\mathbf{w}_{\mathcal{U}} | \mathbf{w}_{\mathcal{S}}) \tilde{p}(\mathbf{w}_{\mathcal{S}}) \prod_{\mathbf{v}_i \in \mathcal{U}} d(\mathbf{w}(\mathbf{v}_i)) \prod_{\mathbf{s}_i \in \mathcal{S}} d(\mathbf{w}(\mathbf{s}_i)) \\ &= \int \tilde{p}(\mathbf{w}_{\mathcal{S}}) \left(\int \tilde{p}(\mathbf{w}_{\mathcal{U}} | \mathbf{w}_{\mathcal{S}}) \prod_{\mathbf{v}_i \in \mathcal{U}} d(\mathbf{w}(\mathbf{v}_i)) \right) \prod_{\mathbf{s}_i \in \mathcal{S}} d(\mathbf{w}(\mathbf{s}_i)) = \int \tilde{p}(\mathbf{w}_{\mathcal{S}}) \prod_{\mathbf{s}_i \in \mathcal{S}} d(\mathbf{w}(\mathbf{s}_i)) = 1 \end{aligned}$$

Note that \mathcal{S} is fixed. Therefore, the expression for the joint density of $\mathbf{w}_{\mathcal{V}}$ depends only on the neighbor sets $N(\mathbf{v}_i)$ for $\mathbf{v}_i \in \mathcal{U}$. Thus, the NNGP density for \mathcal{V} is free of any permutations of locations inside \mathcal{V} proving part (a).

To prove Part (b), let $\mathcal{V}_1 = \mathcal{V} \cup \{\mathbf{v}_0\}$. We split the proof into two cases. If $\mathbf{v}_0 \in \mathcal{S}$, then using the fact $\mathcal{V}_1 \setminus \mathcal{S} = \mathcal{V} \setminus \mathcal{S} = \mathcal{U}$, we obtain

$$\begin{aligned} \int \tilde{p}(\mathbf{w}_{\mathcal{V}_1}) d(\mathbf{w}(\mathbf{v}_0)) &= \int \tilde{p}(\mathbf{w}_{\mathcal{S}}) \tilde{p}(\mathbf{w}_{\mathcal{V}_1 \setminus \mathcal{S}} | \mathbf{w}_{\mathcal{S}}) \prod_{\mathbf{s}_i \in \mathcal{S} \setminus \mathcal{V}_1} d(\mathbf{w}(\mathbf{s}_i)) d(\mathbf{w}(\mathbf{v}_0)) \\ &= \int \tilde{p}(\mathbf{w}_{\mathcal{S}}) \tilde{p}(\mathbf{w}_{\mathcal{V} \setminus \mathcal{S}} | \mathbf{w}_{\mathcal{S}}) \prod_{\mathbf{s}_i \in \mathcal{S} \setminus \mathcal{V}} d(\mathbf{w}(\mathbf{s}_i)) = \tilde{p}(\mathbf{w}_{\mathcal{U}}). \end{aligned}$$

If $\mathbf{v}_0 \notin \mathcal{S}$, then $\mathbf{w}(\mathbf{v}_0)$ does not appear in the neighborhood set of any other term. So, $p(\mathbf{w}(\mathbf{v}_0 | \mathbf{w}_{\mathcal{S}})$ integrates to one with respect to $d(\mathbf{w}(\mathbf{v}_0))$. Part (b) now follows from $\int p(\mathbf{w}_{\mathcal{V}_1} | \mathbf{w}_{\mathcal{S}}) d(\mathbf{w}(\mathbf{v}_0)) = p(\mathbf{w}_{\mathcal{V}} | \mathbf{w}_{\mathcal{S}})$. ■

Proof of Theorem 4: Part (a): Standard Gaussian conditional distribution facts reveal that the conditional distribution $\mathbf{w}(\mathbf{u}_i) | \mathbf{w}_{\mathcal{S}} \sim N(\mathbf{B}_{\mathbf{u}_i} \mathbf{w}_{N(\mathbf{u}_i)}, \mathbf{F}_{\mathbf{u}_i})$. From (4), we see that

$$\tilde{p}(\mathbf{w}_{\mathcal{U}} | \mathbf{w}_{\mathcal{S}}) = \frac{1}{\prod_{i=1}^r \sqrt{\det(\mathbf{F}_{\mathbf{u}_i})}} \exp \left(-\frac{1}{2} \sum_{i=1}^r (\mathbf{w}(\mathbf{u}_i) - \mathbf{B}_{\mathbf{u}_i} \mathbf{w}_{N(\mathbf{u}_i)})' \mathbf{F}_{\mathbf{u}_i}^{-1} (\mathbf{w}(\mathbf{u}_i) - \mathbf{B}_{\mathbf{u}_i} \mathbf{w}_{N(\mathbf{u}_i)}) \right)$$

The rest of the proof is analogous to that of Theorem 2.

Part (b): As $\mathbf{w}_{\mathcal{S}}$ and $\mathbf{w}_{\mathcal{U}} | \mathbf{w}_{\mathcal{S}}$ for every finite \mathcal{U} outside \mathcal{S} has Gaussian density under NNGP, all finite dimensional realizations of an NNGP process will be Gaussian. Let \mathbf{v}_1 and \mathbf{v}_2 be any two locations in \mathcal{D} and let \tilde{E} and \tilde{Cov} denote, respectively, the expectation and covariance operator corresponding to the NNGP. Then, if $\mathbf{v}_1 = \mathbf{s}_i$ and $\mathbf{v}_2 = \mathbf{s}_j$ are both in \mathcal{S} then we obviously have $\tilde{Cov}(\mathbf{w}(\mathbf{v}_1), \mathbf{w}(\mathbf{v}_2) | \boldsymbol{\theta}) = \tilde{\mathbf{C}}_{\mathbf{s}_i, \mathbf{s}_j}$. If \mathbf{v}_1 is outside \mathcal{S} and $\mathbf{v}_2 = \mathbf{s}_j$, then

$$\begin{aligned} \tilde{Cov}(\mathbf{w}(\mathbf{v}_1), \mathbf{w}(\mathbf{v}_2) | \boldsymbol{\theta}) &= \tilde{E}(\tilde{Cov}(\mathbf{w}(\mathbf{v}_1), \mathbf{w}(\mathbf{v}_2) | \mathbf{w}_{\mathcal{S}}, \boldsymbol{\theta})) + \tilde{Cov}(\tilde{E}(\mathbf{w}(\mathbf{v}_1)), \tilde{E}(\mathbf{w}(\mathbf{v}_2)) | \mathbf{w}_{\mathcal{S}}, \boldsymbol{\theta})) \\ \therefore \tilde{\mathbf{C}}(\mathbf{v}_1, \mathbf{v}_2 | \boldsymbol{\theta}) &= 0 + \tilde{Cov}(\mathbf{B}_{\mathbf{v}_1} \mathbf{w}_{N(\mathbf{v}_1)}, \mathbf{w}(\mathbf{s}_j) | \boldsymbol{\theta}) = \mathbf{B}_{\mathbf{v}_1} \tilde{\mathbf{C}}_{N(\mathbf{v}_1), \mathbf{s}_j} \end{aligned}$$

If both \mathbf{v}_1 and \mathbf{v}_2 are outside \mathcal{S} , then $\tilde{\mathbf{C}}(\mathbf{v}_1, \mathbf{v}_2 | \boldsymbol{\theta}) = \delta(\mathbf{v}_1 = \mathbf{v}_2) \mathbf{F}_{\mathbf{v}_1} + \mathbf{B}_{\mathbf{v}_1} \tilde{\mathbf{C}}_{N(\mathbf{v}_1), N(\mathbf{v}_2)} \mathbf{B}'_{\mathbf{v}_2}$, which yields (7).

Part (c): For any two set of locations A and B , let $\|A, B\|$ denote the pairwise Euclidean distance matrix. Since \mathcal{S} is finite, it is easy to verify that $\lim_{\mathbf{h}_i \rightarrow 0} \|(\mathbf{v}_i + \mathbf{h}_i, N(\mathbf{v}_i + \mathbf{h}_i))\| \rightarrow \|(\mathbf{v}_i, N(\mathbf{v}_i))\|$, for $i = 1, 2$, and $\lim_{\mathbf{h}_1 \rightarrow 0, \mathbf{h}_2 \rightarrow 0} \|N(\mathbf{v}_1 + \mathbf{h}_1), N(\mathbf{v}_2 + \mathbf{h}_2)\| \rightarrow \|N(\mathbf{v}_1), N(\mathbf{v}_2)\|$. We prove the continuity of $\tilde{\mathbf{C}}(\mathbf{v}_1, \mathbf{v}_2 | \boldsymbol{\theta})$ for the case when \mathbf{v}_1 is outside \mathcal{S} and $\mathbf{v}_2 = \mathbf{s}_j$. The other cases are proved similarly.

We assume that the covariance function for the original GP is stationary and continuous. The two distance results yield $\mathbf{B}_{\mathbf{v}_1+\mathbf{h}_1} = \mathbf{C}_{\mathbf{v}_1+\mathbf{h}_1, N(\mathbf{v}_1+\mathbf{h}_1)} \mathbf{C}_{N(\mathbf{v}_1+\mathbf{h}_1)}^{-1} \rightarrow \mathbf{C}_{\mathbf{v}_1, N(\mathbf{v}_1)} \mathbf{C}_{N(\mathbf{v}_1)}^{-1} = \mathbf{B}_{\mathbf{v}_1}$. Also, as $\mathbf{v}_2 + \mathbf{h}_2 \rightarrow \mathbf{v}_2 = \mathbf{s}_j$, then $\mathbf{s}_j \in N(\mathbf{v}_2 + \mathbf{h}_2)$ for small enough \mathbf{h}_2 . Let $\mathbf{s}_j = N(\mathbf{v}_2 + \mathbf{h}_2)(1)$ and, hence, $\mathbf{C}_{\mathbf{v}_2+\mathbf{h}_2, N(\mathbf{v}_2+\mathbf{h}_2)} \mathbf{C}_{N(\mathbf{v}_2+\mathbf{h}_2)}^{-1} \rightarrow \mathbf{e}_1$ where $\mathbf{e}_1 = (1, 0, \dots, 0)_{m \times 1}$. Therefore,

$$\begin{aligned} \lim_{\mathbf{h}_1 \rightarrow 0, \mathbf{h}_2 \rightarrow 0} \tilde{\mathbf{C}}(\mathbf{v}_1 + \mathbf{h}_1, \mathbf{v}_2 + \mathbf{h}_2 | \boldsymbol{\theta}) &= \mathbf{B}_{\mathbf{v}_1} \lim_{\mathbf{h}_1 \rightarrow 0, \mathbf{h}_2 \rightarrow 0} \widetilde{\text{Cov}}(\mathbf{w}_{N(\mathbf{v}_1+\mathbf{h}_1)}, \mathbf{w}_{N(\mathbf{v}_2+\mathbf{h}_2)} | \boldsymbol{\theta}) \mathbf{e}_1 \\ &= \mathbf{B}_{\mathbf{v}_1} \lim_{\mathbf{h}_1 \rightarrow 0} \widetilde{\text{Cov}}(\mathbf{w}_{N(\mathbf{v}_1+\mathbf{h}_1)}, \mathbf{w}(\mathbf{s}_j) | \boldsymbol{\theta}) = \mathbf{B}_{\mathbf{v}_1} \tilde{\mathbf{C}}_{N(\mathbf{v}_1), \mathbf{s}_j} = \tilde{\mathbf{C}}(\mathbf{v}_1, \mathbf{v}_2 | \boldsymbol{\theta}). \quad \blacksquare \end{aligned}$$

References

- Banerjee, S., Carlin, B. P., and Gelfand, A. E. (2014), *Hierarchical Modeling and Analysis for Spatial Data*, In press, 2nd ed.
- Banerjee, S., Finley, A. O., Waldmann, P., and Ericsson, T. (2010), “Hierarchical Spatial Process Models for Multiple Traits in Large Genetic Trials,” *Journal of the American Statistical Association*, 105, 506–521.
- Banerjee, S., Gelfand, A. E., Finley, A. O., and Sang, H. (2008), “Gaussian Predictive Process Models for Large Spatial Datasets,” *Journal of the Royal Statistical Society Series B*, 70, 825–848.
- Bechtold, W. A. and Patterson, P. L. (2005), “The Enhanced Forest Inventory and Analysis National Sample Design and Estimation Procedures,” *SRS-80, U.S. Department of Agriculture, Forest Service, Southern Research Station: Asheville, NC*.
- Crainiceanu, C. M., Diggle, P. J., and Rowlingson, B. (2008), “Bivariate Binomial Spatial Modeling of Loa Loa Prevalence in Tropical Africa,” *Journal of the American Statistical Association*, 103, 21–37.
- Cressie, N. and Johannesson, G. (2008), “Fixed Rank Kriging for Very Large Data Sets,” *Journal of the Royal Statistical Society Series B*, 70, 209–226.
- Cressie, N. and Wikle, C. K. (2011), *Statistics for Spatio-Temporal Data*, Wiley-Interscience, 1st ed.
- Davis, T. A. (2006), *Direct Methods for Sparse Linear Systems*, Society for Industrial and Applied Mathematics.
- Du, J., H, Z., and Mandrekar, V. S. (2009), “Fixed-domain Asymptotic Properties of Tapered Maximum Likelihood Estimators,” *Annals of Statistics*, 37, 3330–3361.
- Eidsvik, J., Shaby, B. A., Reich, B. J., Wheeler, M., and Niemi, J. (2014), “Estimation and Prediction in Spatial Models With Block Composite Likelihoods,” *Journal of Computational and Graphical Statistics*, 23, 295–315.

- Finley, A. O., Banerjee, S., and Gelfand, A. E. (2013), “spBayes for large univariate and multivariate point-referenced spatio-temporal data models,” *Journal of Statistical Software*, 0, In press.
- Finley, A. O., Banerjee, S., and McRoberts, R. E. (2009), “Hierarchical Spatial Models for Predicting Tree Species Assemblages across Large Domains,” *The Annals of Applied Statistics*, 0, 1–32.
- Furrer, R., Genton, M. G., and Nychka, D. (2006), “Covariance Tapering for Interpolation of Large Spatial Datasets,” *Journal of Computational and Graphical Statistics*, 15, 503–523.
- Gelfand, A. and Banerjee, S. (2010), “Multivariate Spatial Process Models,” in *Handbook of Spatial Statistics*, eds. Gelfand, A., Diggle, P., Fuentes, M., and Guttorp, P., CRC Press, pp. 495–516.
- Gelfand, A. and Ghosh, S. K. (1998), “Model choice: A Minimum Posterior Predictive Loss Approach,” *Biometrika*, 85, 1–11.
- Higdon, D. (2001), “Space and Space Time Modeling using Process Convolutions,” *Technical Report, Institute of Statistics and Decision Sciences, Duke University, Durham*.
- Kammann, E. E. and Wand, M. P. (2003), “Geoadditive Models,” *Applied Statistics*, 52, 1–18.
- Katzfuss, M. and Cressie, N. (2012), “Bayesian hierarchical spatio-temporal smoothing for very large datasets,” *Environmetrics*, 23, 94–107.
- Kaufman, C. G., Scheverish, M. J., and Nychka, D. W. (2008), “Covariance Tapering for Likelihood-Based Estimation in Large Spatial Data Sets,” *Journal of the American Statistical Association*, 103, 1545–1555.
- Moller, J. and Waagepetersen, R. P. (2003), *Statistical Inference and Simulation for Spatial Point Processes*, Chapman and Hall, 1st ed.
- Rasmussen, C. E. and Williams, C. K. I. (2005), *Gaussian Processes for Machine Learning*, The MIT Press, 1st ed.
- Rue, H. and Held, L. (2004), *Gaussian Markov Random Fields: Theory and Applications*, Chapman and Hall, 1st ed.
- Sang, H. and Huang, J. Z. (2012), “A Full Scale Approximation of Covariance Functions for Large Spatial Data Sets,” *Journal of the Royal Statistical Society: Series B (Statistical Methodology)*, 74, 111–132.
- Schabenberger, O. and Gotway, C. A. (2004), *Statistical Methods for Spatial Data Analysis*, Chapman and Hall/CRC, 1st ed.

- Spiegelhalter, D. J., Best, N. G., Carlin, B. P., and van der Linde, A. (2002), “Bayesian Measures of Model Complexity and Fit,” *Journal of the Royal Statistical Society B*, 64, 583–639.
- Stein, M. L. (1999), *Interpolation of Spatial Data: Some Theory for Kriging*, Springer, 1st ed.
- (2007), “Spatial Variation of Total Column Ozone on a Global Scale,” *Annals of Applied Statistics*, 1, 191–210.
- (2008), “A Modeling Approach for Large Spatial Datasets,” *Journal of the Korean Statistical Society*, 37, 3–10.
- (2013), “Limitations on Low Rank Approximations for Covariance Matrices of Spatial Data,” *Spatial Statistics*.
- Stein, M. L., Chi, Z., and Welty, L. J. (2004), “Approximating Likelihoods for Large Spatial Data Sets,” *Journal of the Royal Statistical Society. Series B (Methodological)*, 66, 275–296.
- Vecchia, A. V. (1988), “Estimation and Model Identification for Continuous Spatial Processes,” *Journal of the Royal Statistical Society. Series B (Methodological)*, 50, 297–312.
- (1992), “A New Method of Prediction for Spatial Regression Models with Correlated Errors,” *Journal of the Royal Statistical Society. Series B (Methodological)*, 54, 813–830.
- Wang, Q., Adiku, S., Tenhunen, J., et al. (2005), “On the Relationship of NDVI with Leaf Area Index in a Deciduous Forest Site,” *Remote Sensing of Environment*, 94, 244–255.
- Yeniay, O. and Goktas, A. (2002), “A comparison of partial least squares regression with other prediction methods,” *Hacettepe Journal of Mathematics and Statistics*, 31, 99–111.
- Zhang, X. and Kondraguanta, S. (2006), “Estimating Forest Biomass in the USA Using Generalized Allometric Models and MODIS Land Products,” *Geophysical Research Letters*, 33, L09402.

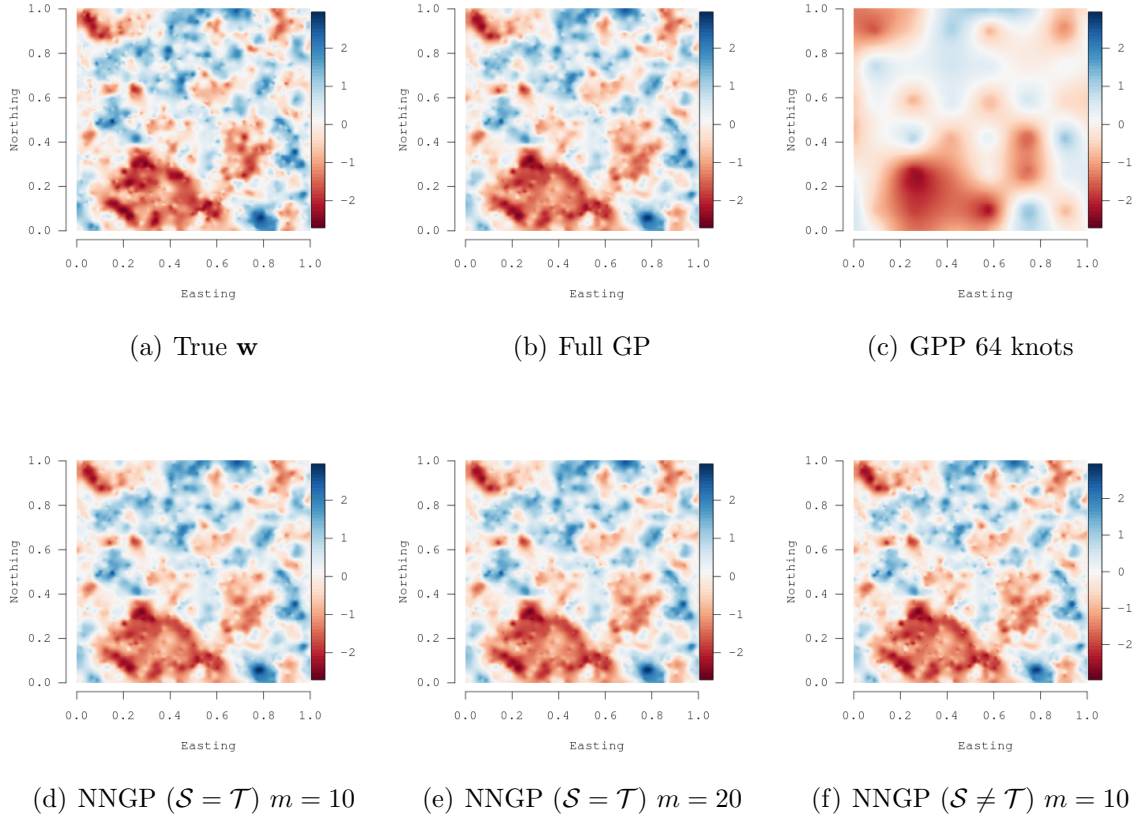
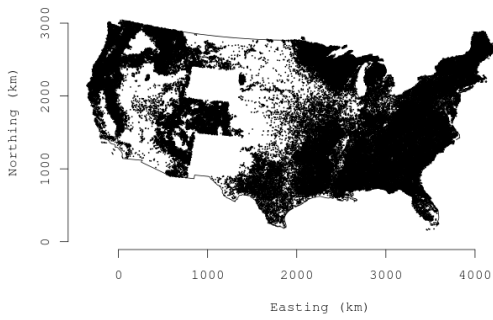
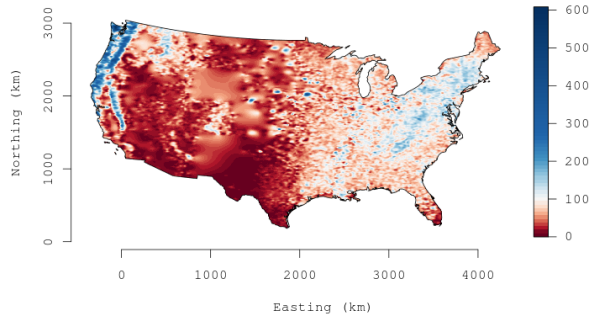


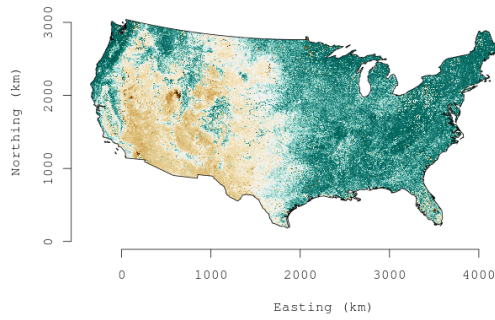
Figure 4: Univariate synthetic data analysis: Figures (a),(b) and (c) shows interpolated surfaces of the true spatial random effects, and posterior median estimates for full geostatistical model and predictive process model (with 64 knots) respectively. Figures (d) and (e) shows interpolated surfaces of the posterior median estimates for NNGP model with $\mathcal{S} = \mathcal{T}$ and $m = 10$ and $m = 20$ respectively. Figure (f) gives the interpolated surface for NNGP ($\mathcal{S} \neq \mathcal{T}$) model with $m = 10$.



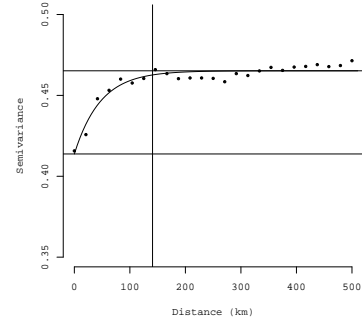
(a) Observed locations



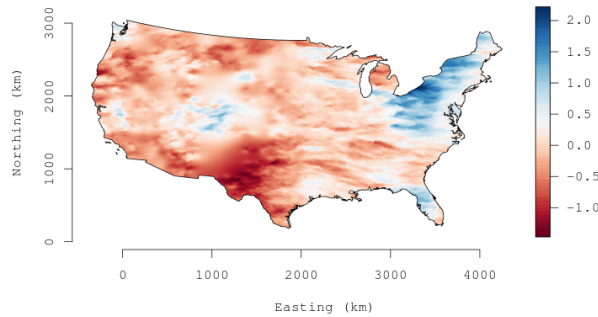
(b) Observed biomass



(c) NDVI



(d) Non-spatial model residuals



(e) SVI $\beta_0(\mathbf{t})$

Figure 5: Forest biomass data analysis locations of observed biomass (a), interpolated biomass response variable (b), and NDVI regression covariate (c). Variogram of non-spatial model residuals (d) and surface of the SVI model random spatial effects posterior medians (e). Following our FIA data sharing agreement, plot locations depicted in (a) have been “fuzzed” to hide the true coordinates.

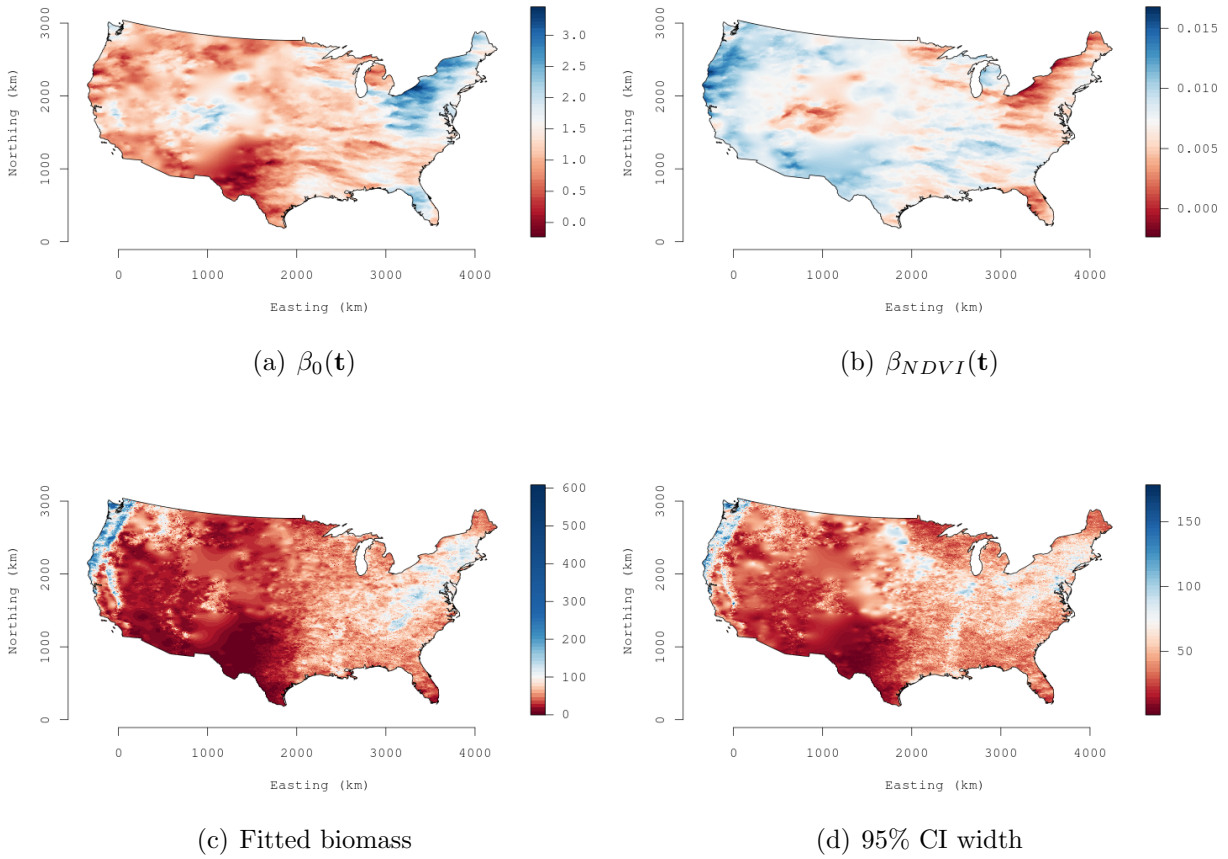


Figure 6: Forest biomass data analysis SVC model posterior medians of the intercept (a) and NDVI (b) regression coefficients. Median of biomass posterior predictive distribution (c) and range between the upper and lower 95% percentiles of the posterior predictive distribution (d).